Renewable Energy 245 (2025) 122728

Contents lists available at ScienceDirect

Renewable Energy

journal homepage: www.elsevier.com/locate/renene

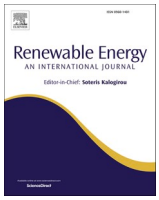

Analysis of a novel PVT dryer using a sustainable control approach

Fazlı Bayrak [a], Mustafa Aktaş [b], Ahmet Aktaş [b], Seyfi Şevik [c,*], Burak Aktekeli [d], Yaren Güven [b]

[a] Graduate School of Natural and Applied Sciences, Gazi University, Ankara, Türkiye
[b] Energy Systems Engineering, Technology Faculty, Gazi University, Ankara, Türkiye
[c] Electrical and Energy, Vocational School of Technical Sciences, Hitit University, Çorum, Türkiye
[d] Worker Health and Safety, Osmaneli Vocational School, Bilecik Şeyh Edebali University, Osmaneli, 11500, Bilecik, Türkiye

ARTICLE INFO

Keywords:
PV
PVT
PVT dryer
Control algorithm
Variable air volume
Apple drying

ABSTRACT

This study aimed to improve a product-focused approach for enhancing electrical and drying efficiency by utilizing a novel photovoltaic thermal (PVT) collector and a temperature control algorithm, as opposed to existing fixed implementations. Apple slices were dried in the variable air volume PVT dryer (VAVPVTD) and constant air volume PVT dryer (CAVPVTD) for desirable drying efficiency at varying air velocities. The performance of the VAVPVTD, which provides homogeneous cooling with the novel design and controls the air volume according to the surface temperature of the PV with the created algorithm, was compared to the CAVPVT. While the average surface temperature of PVT in high air volume CAVPVTD (CAVPVTD-HAV) was 5.76 % and 5.63 % lower daily, respectively, the values in VAVPVTD were 7.15 % and 4.26 % lower compared to CAVPVTD. The maximum electrical efficiency was found to be 12.51 %, 11.96 %, and 12.57 % on days 1, 3 and 4, respectively. In terms of average thermal efficiencies, Day 3's highest value was 39.05 % in CAVPVT, while Day 3's lowest value was 28.67 % in VAVPVT. Although VAV control significantly increases the electrical efficiency in PVT, the thermal efficiency was lower compared to CAVPVT. Despite the uniform temperature distribution and the favorable impact of the VAV control application on electrical efficiency, thermal efficiency was adversely impacted based on the temperature that was chosen.

1. Introduction

Drying of agricultural products faces problems such as high energy costs and the quality of the dried product. Utilizing sustainable solar dryers can save energy costs and the amount of fossil fuels used in the drying process of agricultural products, which is energy-intensive [1]. The use of solar energy in drying processes increases the rate of renewable energy use in the agricultural sector, while at the same time providing a sustainable production and consumption model [2,3].

Drying is a process often used for food preservation [4]. For drying systems, manufacturers want the product to dry in less time, meet the appropriate quality criteria, and reduce the cost of equipment and energy. Photovoltaic thermal (PVT) collectors are hence suitable for drying applications. PVTs can provide all the heat and electricity for drying from the sun [3]. Recently, researchers have been focusing on PVT drying systems because PVT systems can produce both heat and electricity [5–15]. Barnwal and Giwari [5] dried green premature and yellow fully mature grapes in both open air and a hybrid PVT greenhouse dryer. The drying time of fully mature grapes was shorter than that of premature grapes. The moisture evaporated is more in open conditions than in greenhouse conditions due to a rate of heat evaporated for a higher value of wind velocity and its combined effect with relative humidity. However, they stated that this situation could be overcome with high airflow rates. Kong et al. [6] dried fresh turnips in two different PVTs with direct current (DC) fans. The average thermal efficiency and average electrical efficiency of amorphous silicon PVT were 46.8 % and 5.7 %, respectively. The average thermal efficiency and average electrical efficiency of polysilicon PVT were 40.7 % and 6.8 %, respectively. By increasing the number of fans, they shortened the drying time by 10 h. Fterich et al. [7] developed a numerical simulation to investigate the effects of drying temperature, slice thickness, and air-drying rate on the heat and mass transfer distribution in tomato slices in a PVT dryer and tested experimentally. Gupta et al. [8] developed a PVT dryer for drying green tea and investigated the effects of mixed

* Corresponding author.
E-mail addresses: bayrak.fazli@gmail.com (F. Bayrak), mustafaaktas@gazi.edu.tr (M. Aktaş), a.aktas@gazi.edu.tr (A. Aktaş), seyfisevik@hitit.edu.tr (S. Şevik), burak.aktekeli@bilecik.edu.tr (B. Aktekeli), yarenguven@gazi.edu.tr (Y. Güven).

https://doi.org/10.1016/j.renene.2025.122728
Received 19 October 2024; Received in revised form 19 February 2025; Accepted 19 February 2025
Available online 22 February 2025

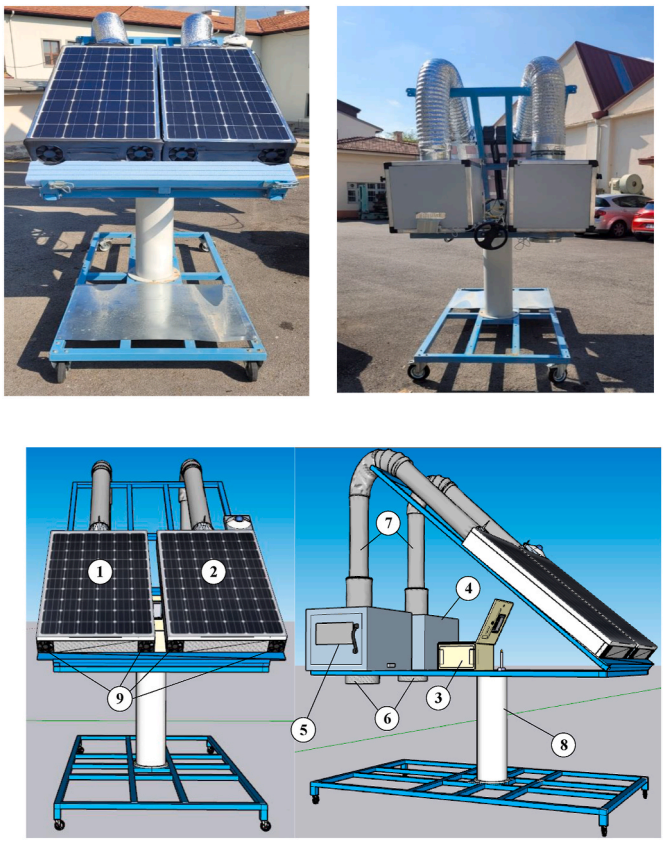

Fig. 1. Photograph and schematic of the VAVPVTD and CAVPVTD systems. 1: VAVPVT, 2: CAVPVT, 3: Automation panel, 4: Drying chamber (CAVPVTD), 5: Drying chamber (VAVPVTD), 6: Drying room outlet air, 7: PVT outlet air/drying room inlet air, 8: Platform, 9: Fans.

mode and indirect mode natural convection, and forced convection on PVT performance. They achieved optimum drying performance in mixed mode with average PVT drying efficiency and specific moisture extraction rate (SMER) of 26.34 % and 0.3560 kg/kWh, respectively. They also found the maximum value of PVT collector efficiency to be 39.67 % in mixed mode. A PVT dryer was developed by Gupta et al. [9] to dry green chilies. The PVT dryer's thermal energy, electrical energy, and total thermal energy for the 8 h of the experiment were 0.409, 0.859, and 1.933 kWh/day, respectively. Furthermore, the PVT solar dryer was found to have an average electrical efficiency of 12.29 %, a thermal efficiency of 18.81 %, and an overall thermal efficiency of 51.18 %. Dorouzi et al. [10] developed a liquid desiccant-assisted solar dryer with a PVT regeneration system and tested it by drying tomatoes. The highest electrical energy consumption was observed at 28 % relative humidity and 70 °C temperature. They found that the solar electricity-to-electricity consumed ratio was about 2.2 times higher when tomatoes were dried at 60 °C instead of 70 °C. Gupta et al. [11] conducted an environmental and economic evaluation of the designed PVT dryer and found the electrical, thermal, and overall thermal efficiencies to be 12.99 %, 50.79 %, and 84.99 %, respectively. Additionally, the energy payback period of the PVT dryer was estimated at 1.45 years.

Kong et al. [12] developed a hybrid drying system powered by PVT, wind turbine, dried the main root, rhizome, and fibrous root of Panax notoginseng, and compared it with open-air drying. Drying time was shortened by 33.3 % for main root slices, 74.1 % for rhizomes, and 53.8 % for fibrous roots compared to open-air drying. They also calculated the payback period of the hybrid dryer as approximately 1.03 years. Tiwari et al. [13] developed a mixed-mode PVT greenhouse solar dryer and dried grapes. They covered the entire roof of the dryer with

Table 1
Characteristics of equipment and measuring instruments used in the PVTD systems.

Equipment	Features	Accuracy
PV	Monocrystalline 36 cells, Power: 100 W, surface area: 0.65 $m^2 \times 2 = 1.3\ m^2$	±3 %
Plates	Aluminum, area: 0.51 m^2, dimensions of unperforated plates: 800 × 150 mm, dimensions of perforated plates: 900 × 150 mm, thickness: 0.5 mm	–
Insulated PVT back surface sheet	Aluminum sheet and insulation material, area: 0.65 $m^2 \times 2 = 1.3\ m^2$, insulation material thickness: 20 mm	–
Cooler fans	Voltage: 12 V, current: 0.32 A, dimensions: 12 × 12 × 3.8 cm, speed levels: 0.88–1.63 m/s	–
Pyranometer	0–2000 W/m^2, sensitivity: 5–20 μV/W/m^2, nonlinearity (0–1000 W/m^2): <1 %	< ±5 W/m^2
Temperature sensor	NTC type, resistance value: 10 KΩ ±1 % at 25 °C, operating temperature range: −30 ~ +105 °C	±0.1 °C
Velocity and temperature meter	NTC sensor, temperature range: −20 ~ +70 °C, speed: 0–20 m/s	±0.01 m/s, ±0.1 °C
Thermohygrometer	Temperature range: −20 ~ +55 °C, relative humidity: 0–100 %	T: ±0.4 °C, Rh: ±2 %
Loadcell	Capacity: 10 kg, maximum platform size: 250 × 350 mm, Voltage 5–12V, input resistance 406 Ω ± 6, output resistance 350 Ω ± 3, operating temperature: −35 ~ + 65 °C	≤± 0.015
Loadcell sensor signal amplifier	Supply voltage: 24V, signal input: 1 mV/V, output signal: 0–5V/0–10V/4–20 mA	–
Precision scale	Capacity: 0–6100 g, operating temperature and humidity: 15 − 30 °C and 10–85 % Rh	±0.01 g

photovoltaics and placed extra glass under the photovoltaic module. In this way, the heat transfer coefficient from the product to the environment and the solar irradiation to the product was reduced, resulting in slowly heating of the product and increasing its quality. Fterich et al. [14] dried tomatoes in a forced convection PVT dryer. The moisture content of tomatoes dried at 65 °C decreased from 91.943 % to 22.32 %. The thermal efficiency of PVT ranged between 26 and 65 % and electrical efficiency between 7.5 and 12.31 %.

As can be understood from the above literature, PVT dryers are observed to dry different products effectively. Studies have focused particularly on tomato drying. Apple is a popular fruit widely grown around the world. The shelf life of fresh apples can be extended by using the drying process [15]. Apples can be dried using a variety of methods to retain their original qualities. Once dried, the apples can be consumed or processed to make secondary raw materials [4]. In the existing studies, apple slices were dried at different drying air temperatures at a drying air velocity of 1.5 m/s. Apple slices were dried in a solar air dryer with a sun tracking system at 45 °C [16], in a convection hot air dryer at 50–70 °C [17], and in a cyclone dryer at 60–80 °C [18]. According to studies, the ideal drying temperature can be determined as 40 °C at a drying air velocity of 1.5 m/s, which is also taken into account in the current study.

Although apple drying [15–18] is also among the popular dried products like tomato drying, to our knowledge, apples have not been dried in a dryer using PVT with variable or constant air volume. Baysan et al. [19] applied intermittent drying and humidity-based controlled temperature control methods that prioritize maximum energy efficiency. Although there was an improvement in dried product quality, neither method was effective in maximum energy efficiency. Laskar et al. [20] optimized the drying efficiency of bananas in a microwave dryer using mathematical modeling and regression analysis. They only provided information about the slice geometry and which model was suitable. Despite abundant research on air-cooled PVT systems and PVT

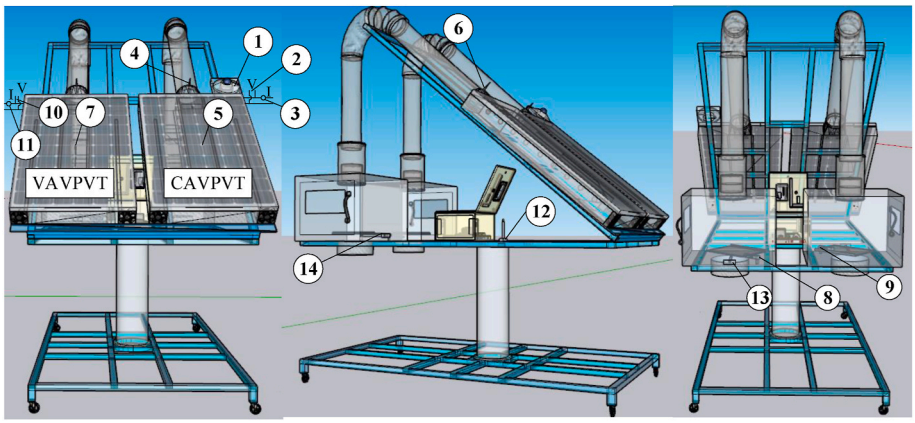

Fig. 2. Illustration of measurement points.
1: Pyrometer, 2: CAVPVT voltage sensor, 3: CAVPVT current sensor, 4: CAVPVT outlet air temperature, 5: CAVPVT surface temperature, 6: VAVPVT outlet air temperature, 7: VAVPVT surface temperature, 8: Loadcell sensor (CAVPVT), 9: Loadcell sensor (VAVPVT), 10: VAVPVT voltage sensor, 11: VAVPVT current sensor, 12: Ambient air temperature and relative humidity sensor, 13: Drying room outlet air temperature and relative humidity sensor (CAVPVT), 14: Drying room outlet air temperature and relative humidity sensor (VAVPVT).

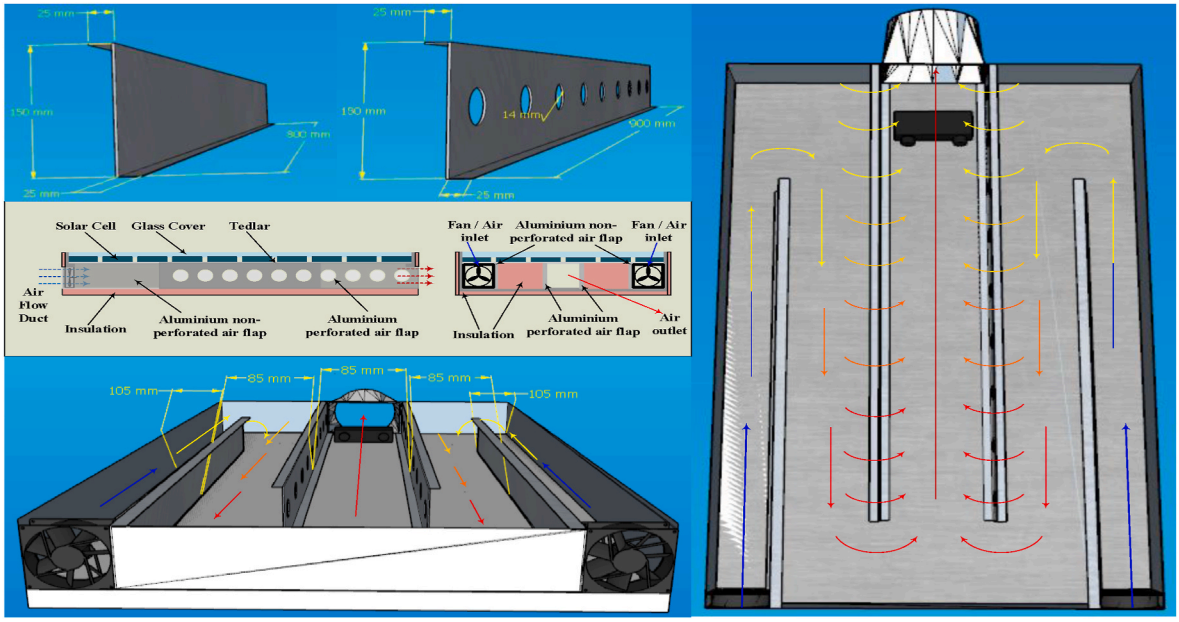

Fig. 3. Detailed illustrations of the air path and fin structure of PVTs.

dryers, no studies have evaluated an approach focused on electric-drying efficiency with an absorber that provides a homogeneous air path with multiple fan and plate placement. In the literature, there is no study on drying apples with a PVT collector with constant air volume and variable air volume. Accordingly, the objectives of this experimental study can be summarized as follows.

- to design and test a novel PVT,
- to investigate the drying kinetics of two different PVT dryers
- to analyze the effect of the constant and variable air volume PVT for energy and drying performance,
- to determine the drying time and drying kinetics of apples utilizing a novel PVT and algorithm,
- to reduce drying time without sacrificing product quality.

It is thought that this design will contribute to the drying sector to dry products with variable air volume depending on temperature without compromising product quality.

2. Material and method

2.1. Experimental setup

The experimental set was installed on a platform with a constant air volume PVT dryer (CAVPVTD) and a variable air volume PVT dryer (VAVPVTD). Fig. 1 shows the photograph and schematic of the VAVPVTD and CAVPVT systems. Each system is prepared identically. The experimental setup consists of monocrystalline PV with 36 cells, fans, a drying chamber, an automation panel, and a platform. The equipment used is given below the figure. Characteristics of equipment and measuring instruments used in the photovoltaic thermal dryer (PVTD) systems are given in Table 1.

Fig. 2 shows the measurement points. The sensors are placed as shown in the figure to measure values such as solar irradiation, temperature, humidity, weight, voltage, and strain. The electrical performance of the photovoltaic (PV) panels was determined by continuously measuring the open circuit voltage (V_{oc}) and short circuit current (I_{sc}).

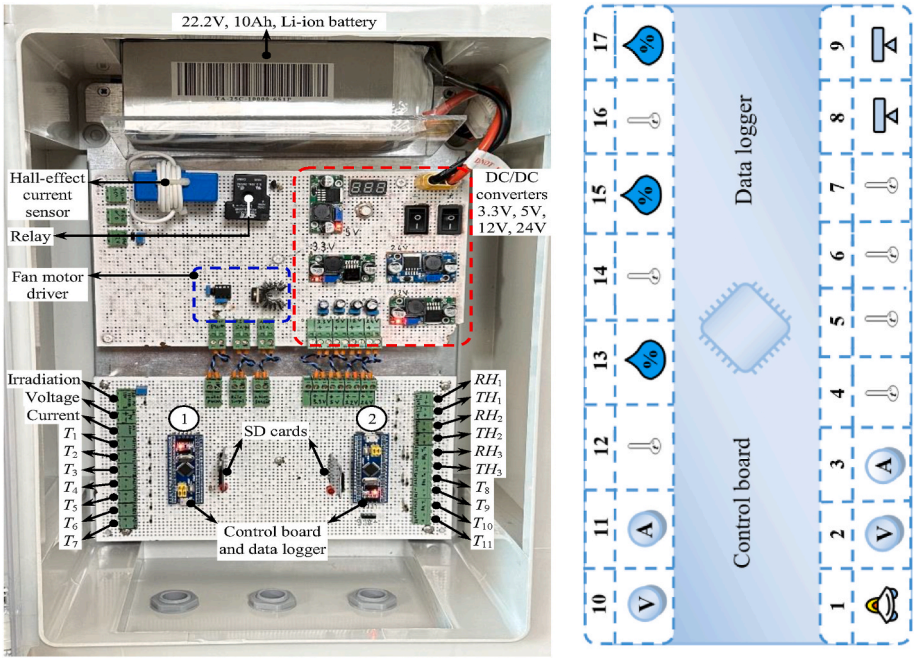

Fig. 4. Control board and datalogger circuits in the PVT systems.

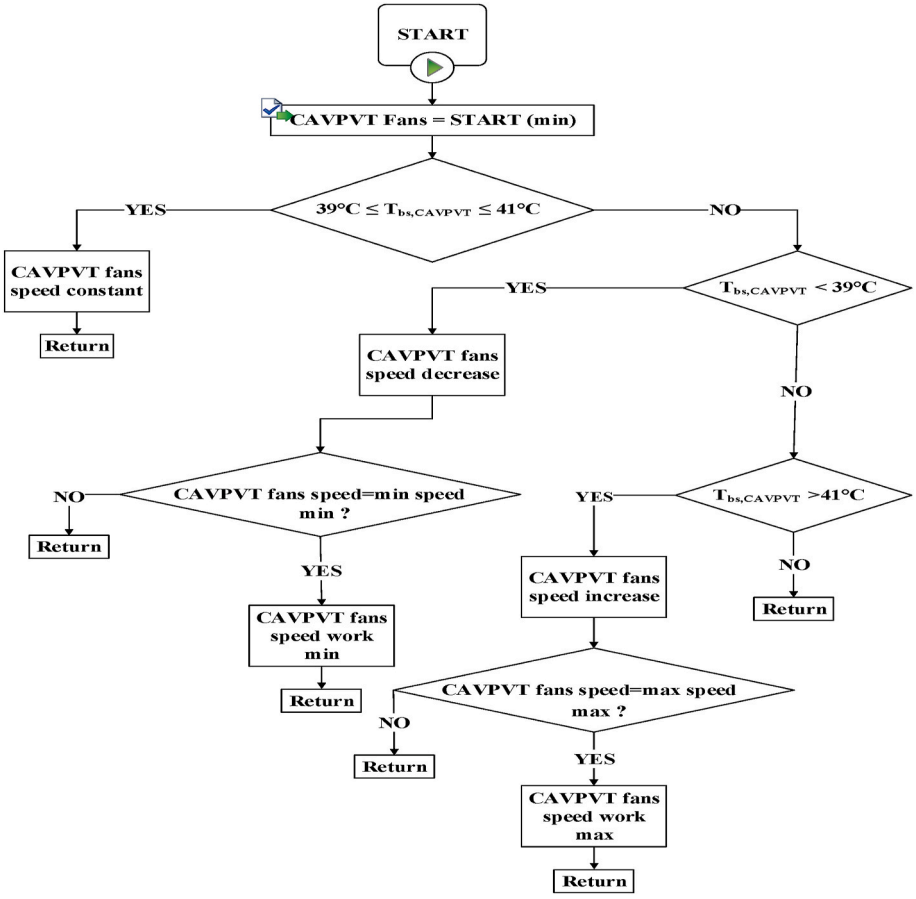

Fig. 5. The flowchart of the CAVPVT system control algorithm.

The electrical performance of the PV panels was measured and calculated using the fill factor (FF) coefficient following the electrical data published by the manufacturer before the experiment. The FF coefficient of the PV panels used in the experimental studies was determined as 0.812 by both the manufacturer and preliminary test studies. During the experiments, the measured V_{oc} and I_{sc} values of the PV panels were

Table 2
Measuring points in systems.

Measurement point	Measurement symbol	Explanation
1	S_{irr}	Solar irradiation
2	v_{CAVPVT}	CAVPVT voltage
3	i_{CAVPVT}	CAVPVT current
4	$T_{ao,CAVPVT}$	CAVPVT air outlet temperature
5	$T_{bs,CAVPVT}$	CAVPVT back surface temperature
6	$T_{ao,VAVPVT}$	VAVPVT air outlet temperature
7	$T_{bs,VAVPVT}$	VAVPVT back surface temperature
8	LC_{CAVPVT}	CAVPVT load cell (measurement mass of material)
9	LC_{VAVPVT}	VAVPVT load cell (measurement mass of material)
10	v_{VAVPVT}	VAVPVT voltage
11	i_{VAVPVT}	VAVPVT current
12	T_{aa}	Ambient air temperature
13	RH_{aa}	Ambient air relative humidity
14	$T_{co,VAVPVT}$	VAVPVT cabinet outlet air temperature
15	$RH_{co,\ VAVPVT}$	VAVPVT cabinet outlet air relative humidity
16	$T_{co,CAVPVT}$	CAVPVT cabinet outlet air temperature
17	$RH_{co,\ CAVPVT}$	CAVPVT cabinet outlet air relative humidity

Table 3
Experimental procedure.

Test days	System-1 (CAVPVTD)	System-2 (VAVPVTD)	Outdoor conditions (Avg.)	Description
	Air velocity (m/s)			
Day-1	1.18	1.63	968.35 W/m^2, 28.19 °C	Both systems are at constant air volume.
Day-2	1.18	1.63	956.96 W/m^2, 28.77 °C	Both systems are at constant air volume.
Day-3	1.18	Variable air volume	957.05 W/m^2, 29.73 °C	While one of the systems is at a constant air volume rate, the other one's volume rate changes depending on the 40 °C PV surface temperature.
Day-4	1.18	Variable air volume	976.56 W/m^2, 31.76 °C	While one of the systems is at a constant air volume rate, the other one's volume rate changes depending on the 40 °C PV surface temperature. Compared to the third day, the outside temperature is higher.

multiplied by FF, and the electrical performance at the maximum power point tracking (MPPT) point was calculated. Thus, the maximum power that can be obtained from the PV panels at the MPPT point was obtained. The FF and MPPT points were determined by using the I-V curve method in the preliminary experiments. While performing the actual experiments, the MPPT point on the I-V curve was determined and recorded with the instantly measured I_{sc} and V_{oc}. The forced air fluid absorbs and removes heat from the PVT panel, thus generating useful heat energy, which increases overall efficiency. Thermal efficiency is calculated using temperature, flow, and radiation data from the datalogger.

Fig. 3 shows comprehensive PVT illustrations. Two fans were used in each PVT and mounted on the right and left sides. While the fans in the CAVPVTD were set to operate at set values, the fans in the VAVPVTD were arranged to operate at variable volumes according to the temperature of a certain area. By sealing the PVT design's rear surface, air tightness between the absorber plates was accomplished. One of the PVTs is closed only at the back. The back of the other PVT has a labyrinth structure consisting of five compartments and extending the air path. Two of the aluminum sheets forming the compartments are perforated and two are flat sheets. The perforated sheets are located in the middle of the PVT, while the flat sheets are located near the edges of the PVT. Thus, when the air is pressed behind the PVT with the help of fans, the air moves towards the upper area of the PVT along the flat sheet and the case, then turns and some of the air moves towards the area where the fans are, then moves towards the upper area of the PVT, combines with the air passing through the holes and leaves the PVT.

2.2. Control algorithm

The control and datalogger boards have a 12-bit analog-to-digital converter (ADC) resolution and are powered by dual STM32F103C8T6 processors. These boards enable the measurement of up to 20 distinct sensor parameters. Fig. 4 shows the topology of the control board and datalogger circuits in the PVT systems. The datalogger collects data such as solar irradiation (with a Kipp&Zonen brand SMP22 pyranometer), current (with a LEM brand LA 200-P hall-effect sensor), and temperature (with negative temperature coefficient (NTC) and thermocouples), and the control board displays them. The relative humidity of the environment was measured using the humidity and temperature sensors from the Notion Control brand. The control board logs the measured data on secure digital (SD) cards once every minute. Fig. 5 shows the flowchart of the proposed control algorithm for the CAVPVT system.

Although both systems were operated at constant volume for two days (Day-1 and Day-2), an algorithm was developed to guarantee that the drying air temperature should not rise above 40 °C to maintain the quality of the apples during drying. However, in this study, the algorithm focused on keeping the PV surface temperature at a certain level. The main goal of the algorithm is to keep the PV efficiency at maximum value by trying to keep the PV temperature at the specified value. Thus, drying processes were carried out depending on the PV surface temperature. Data was collected from the measurement points in Table 2 with the prepared control board and datalogger.

2.3. Preparing the apples

Product quality, which is one of the important criteria in drying systems, is affected by parameters such as chemical deterioration, color changes, absence of contamination and contamination during drying, and fast and simple hydration. Oxygen in the air causes sliced apples to turn brown, meaning enzymatic browning (an oxidation reaction) occurs. Heat and acids are used to prevent this, which is what heat was used in this study. In this study, the products were dried naturally by allowing them to turn brown without any pretreatment. Apples purchased from a local market were washed, dried, sliced, and placed on the shelves. Sliced fresh apples with a weight of 250 g ± 0.5 g and a thickness of 4 mm ± 0.25 mm were utilized in each trial.

2.4. Experimental procedure

Factors affecting the drying velocity are drying air temperature, relative humidity, properties of the product to be dried, product stack thickness, heat transfer method, geometry of the drying chamber, and product mobility [1]. In drying applications, the drying air velocity is significant. In drying applications, drying air velocity is as important as drying temperature. If the drying air velocity is not adjusted according to the product to be dried, deformations may occur while the drying time changes.

The experiments were carried out in an area allocated for experimental studies at the campus of the Faculty of Technology, Gazi University, Ankara, Türkiye. The experimental set was installed on a portable platform that allowed the PVT angle and direction to be changed. The PVTs were placed on the platform at a 36° tilt angle and facing south. The experimental set was safely kept in place without

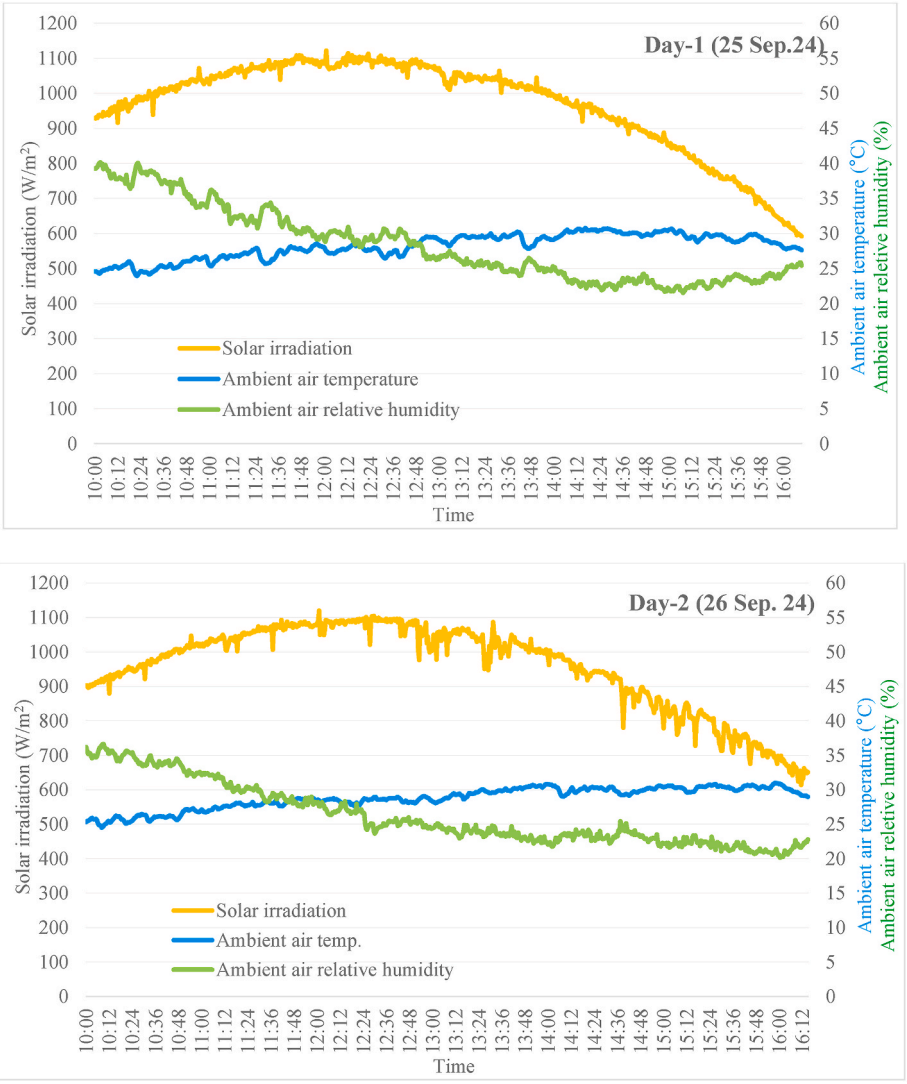

Fig. 6. Graphical representations showing the environmental parameters during the tests.

being moved for the following experiment once the experiments were finished (at the end of the day). Experiments were conducted on four consecutive days in September 2024. The experimental procedure is given in Table 3. Tests are conducted at constant air velocities on the first and second days. One of the systems is operated at a low constant air velocity while the other is operated at a higher constant air velocity. On the third and fourth days, one of the systems is operated at constant air velocity. In contrast, the other is operated at variable air volume depending on the PV surface temperature.

3. Theoretical analysis

In the design of PVT systems, the system's overall performance is evaluated by calculating the efficiency of both PV (η_{PV}) and thermal (η_{th}) components. Accordingly, the sum of these two efficiencies gives the total efficiency (η_{PVT}) of the PVT system [21]:

$$\eta_{PVT} = \eta_{PV} + \eta_{th} \tag{1}$$

The efficiency of the PV panel is found by the ratio of the output power (P_{PVout}) of the panel to the input power (P_{PVin}). This efficiency evaluates the capacity of the PVT system to generate electricity. The efficiency of the PV panel is calculated by the following [22]:

$$\eta_{PV} = \frac{P_{PVout}}{S_{irr} \times A_{PV}} \times 100 \tag{2}$$

Thermal efficiency indicates how effectively the thermal components of the PVT system utilize the incoming solar energy. Thermal efficiency is given below [23]:

$$\eta_{TH} = \frac{\dot{Q}_{th}}{S_{irr} \times A_{PV}} \tag{3}$$

where $\dot{Q}_{th}$ is the thermal energy power collected, S_{irr} is the incoming solar irradiation, and A_{PV} is the PV collector's surface area.

The thermal power of the PVT system is calculated with Eq. (4). Specific heat capacity determines how much energy the fluid in the

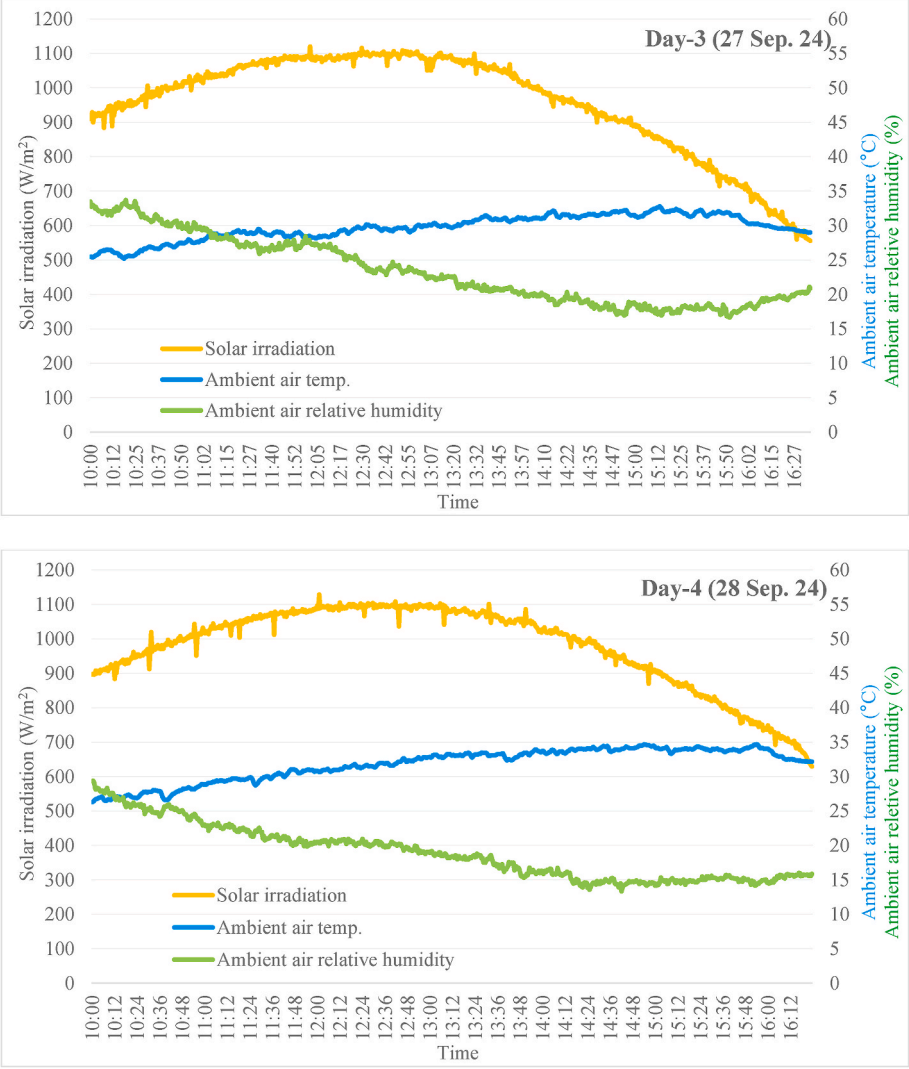

Fig. 6. (*continued*).

system can carry per a given temperature rise. This is a critical component of thermal design and is calculated by Eq. (5) [23,24]:

$$\dot{Q}_{th} = \dot{m} \times c \times (T_{out}\text{-}T_{in}) \tag{4}$$

$$c = \frac{\dot{Q}_{th}}{\dot{m} \times (T_{out}\text{-}T_{in})} \tag{5}$$

where, $\dot{m}$ represents the mass of the fluid, T_{out} and T_{in} are PVT systems inlet and outlet air temperature, c is the specific heat capacity of air under constant pressure, respectively.

Determining the air density in the system is necessary to understand fluid dynamics. The density of air entering the PVT system is calculated by Eq. (6). This equation calculates the fluid's air density under a given temperature and pressure [25]:

$$\rho_{air} = \frac{P_{air}}{R \times (T_{in} + 273.15)} \tag{6}$$

where; P_{atm} is the atmospheric pressure and is used as 101325 N/m^2 in the study, and R is the gas constant of the air and is used as 287 J/kg K in the study.

In drying experiments, the calculation of the moisture content of the products according to the wet basis is made with the following equation [26]:

$$MC_{wb} = \frac{W_w\text{-}D_w}{W_w} \tag{7}$$

where, MC_{wb} represents the moisture content according to a wet basis, W_w and D_w wet weight and dry weight of the product, respectively.

The mass of evaporated water is calculated by the following equation [27]:

$$m_{water} = W_w\text{-}D_w \tag{8}$$

Moisture ratio (MR) refers to the incomplete moisture change in the substance. During drying experiments was calculated using the following equation [28]:

$$MR = \frac{M\text{-}M_e}{M_0\text{-}M_e} \tag{9}$$

where M is the moisture content, M_e is the equilibrium moisture content, and M_o is the initial moisture content, respectively.

Drying rate (DR) is the change in moisture content of the product per unit time interval. It is calculated in drying processes taking into account varying drying rates. The drying rate of the products over-drying experiments can be estimated utilizing the following equations [29]:

$$DR = \frac{M_{t+dt}\text{-}M_t}{d_t} \tag{10}$$

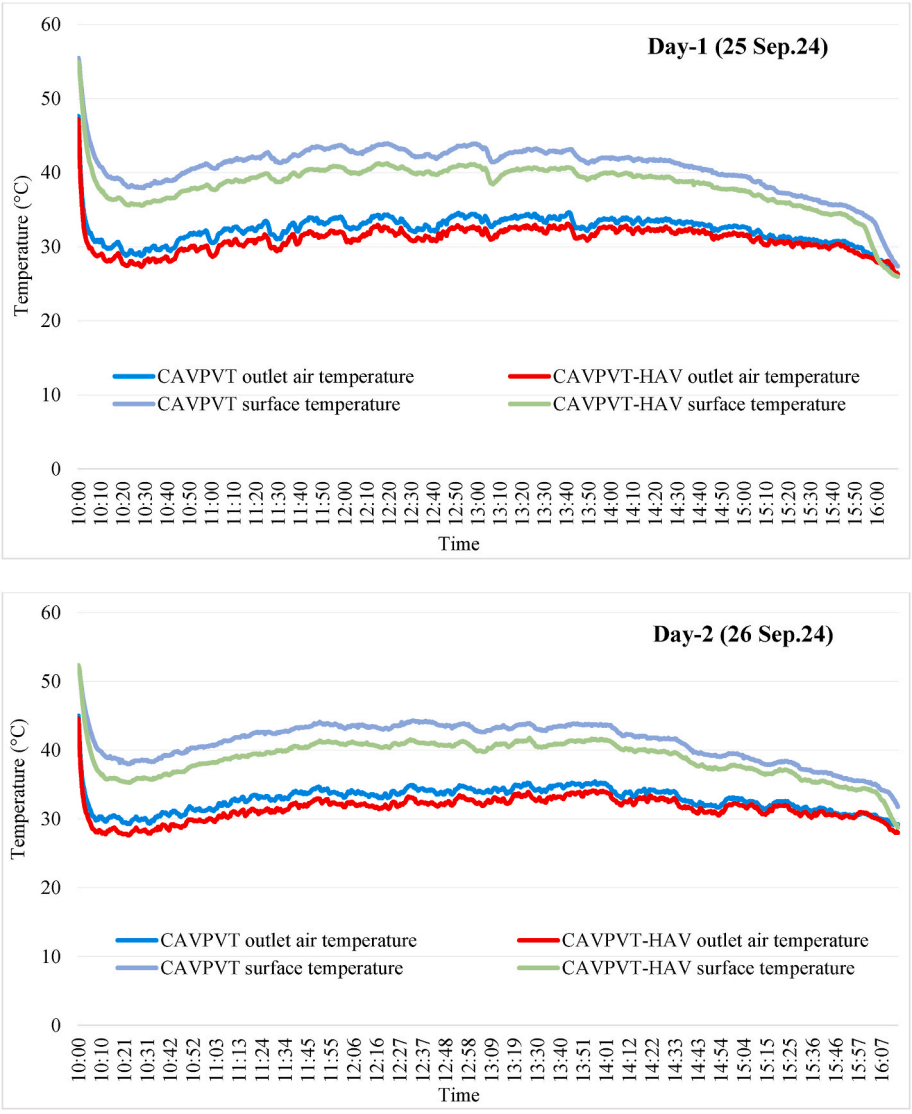

Fig. 7. Instantaneous variation in outlet air temperatures and PVT surface temperatures.

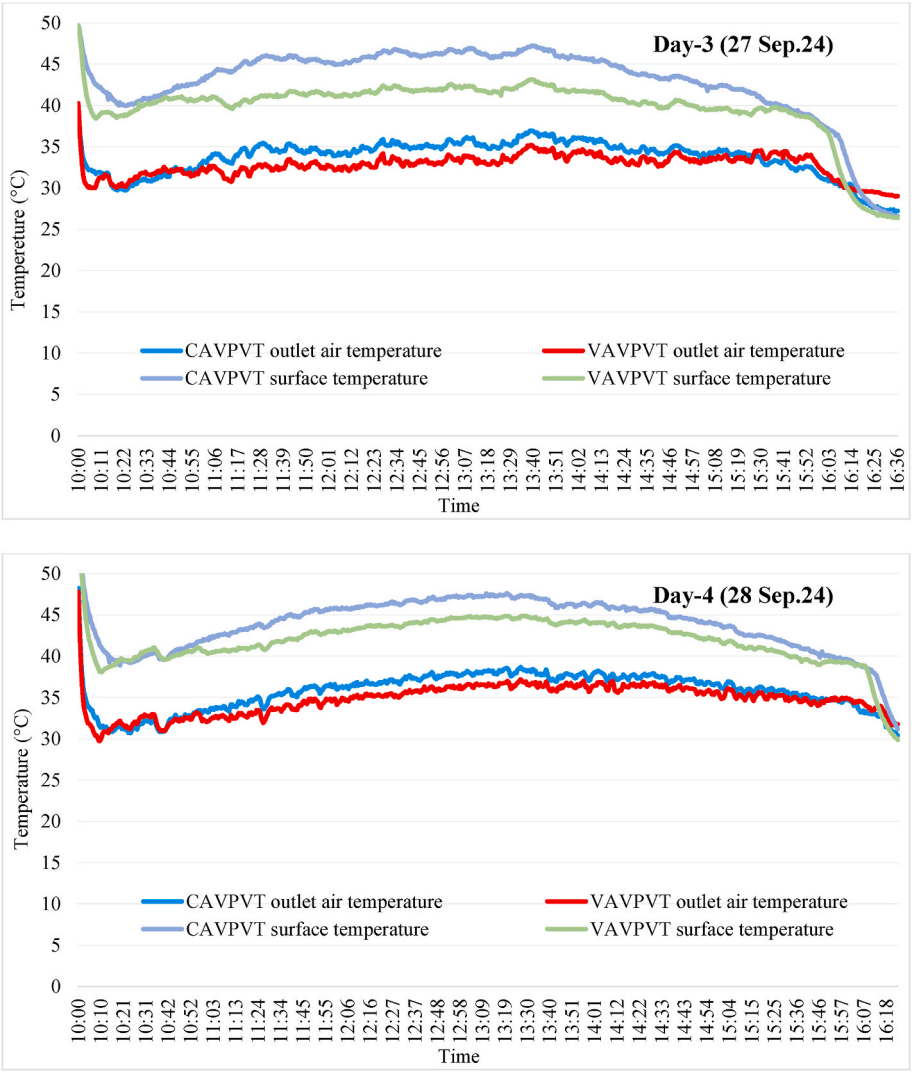

Fig. 7. (*continued*).

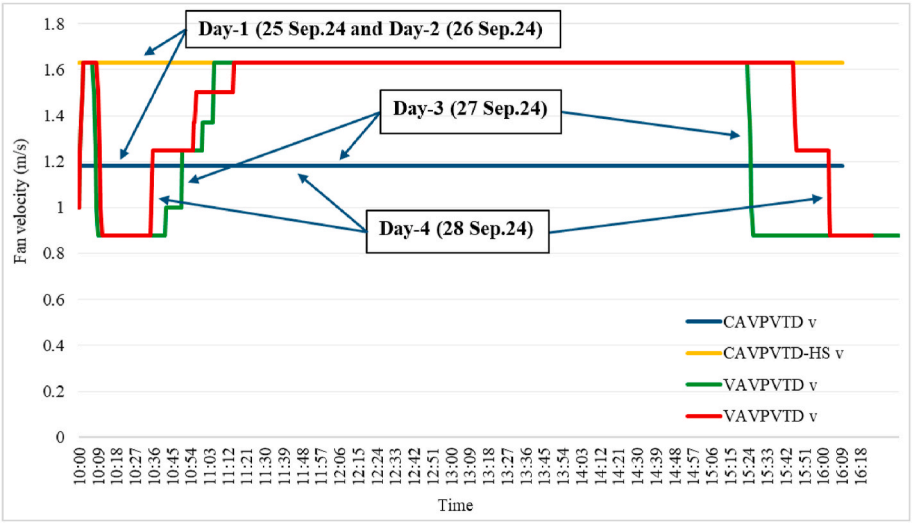

Fig. 8. Instantaneous variation of air velocity.

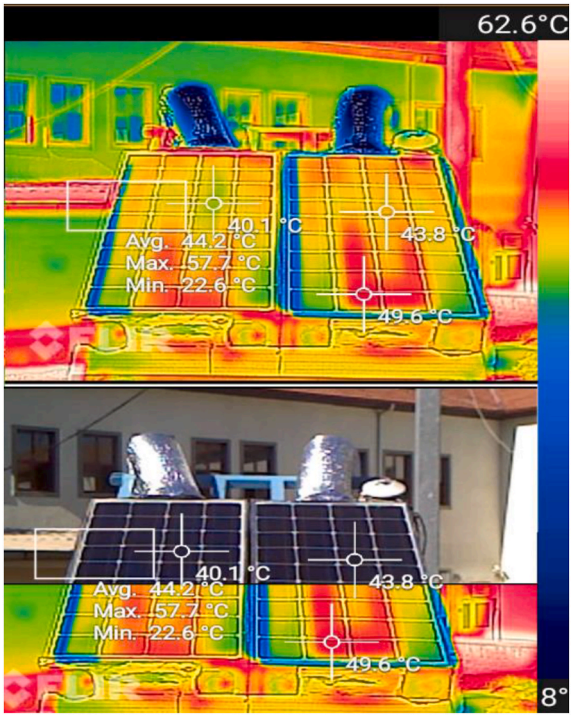

Fig. 9. Images of the thermal camera taken on the Day-4.

where M_{t+dt} is the moisture content at the time "$t + dt$", M_t is the moisture content at the time "t", respectively.

Drying efficiency is calculated by the following equation:

$$\eta_{drying} = \left(\dot{m}_b x h_{fg}\right) / \dot{Q}_{TH} \tag{11}$$

where η_{drying} is the drying efficiency, $\dot{m}_b$ is the mass flow rate measured from loadcell, h_{fg} is the latent heat of vaporization, respectively.

The latent heat of vaporization (h_{fg}) can be calculated at the saturation condition by an equation developed. Two equations are used for h_{fg} as the function of absolute temperature [30]:

$$h_{fg} = 2.503x10^6\text{-}2.386x10^3(T_{da}\text{-}273.16) \text{ if; } 273.16 \le T_{da}(K) \le 338.72 \tag{12}$$

$$h_{fg} = \left(7.33x10^{12}\text{-}1.60x10^7 {T_{da}}^2\right)^{0.5} \text{ if; } 338.73 \le T_{da}(K) \le 533.16 \tag{13}$$

To analyze the flow type, the Reynolds number (Re) can be calculated with the following equation [31]:

$$Re = \frac{V\,L}{\nu} \tag{14}$$

In this equation, V is the mean velocity of air blown to the product whereas L represents the characteristic dimension equal to the internal diameter of the circular drying chamber, and ν is the kinematic viscosity.

Schmidt number (Sc) is determined based on the ratio of momentum diffusivity to mass diffusivity. The Sherwood number (Sh) is defined based on the ratio of mass transfer resistance to the diffusivity. The relationship between convective mass transfer coefficient (h_m), Sh, and Sc [31]:

$$Sc = \frac{\nu}{D_{AB}} \tag{15}$$

$$Sh = 0.037\left(Re^{0.8}\right) Sc^{1/3} \tag{16}$$

$$h_m = \frac{Sh\,D_{AB}}{L} \tag{17}$$

where D_{AB} is the thermal diffusion coefficient.

The partial pressure of water vapor in moist air (P_b) is calculated by the following equation [32]:

$$P_b = P_{d.b}\phi \tag{18}$$

The mass transfer rate of vapor is calculated by the following equation [33]:

$$\dot{m}_{water} = \left(\frac{h_m}{RT}\right)(P_d\text{-}P_b) \tag{19}$$

Drying time is calculated by the following equation [27]:

$$t = \frac{m_{water}}{\dot{m}_{water}} \tag{20}$$

The specific moisture extraction rate ($SMER$) value represents the amount of energy used to get rid of 1 kg of water from the product. The consumption of total power for the dryer may be related to the energy supplied by the PV. The $SMER$ can be calculated with the following equation [34]:

$$SMER = \frac{\dot{m}_{water}}{P_{PVin}} \tag{21}$$

The coefficient of performance (COP) is the ratio of useful thermal energy to energy consumption.

$$COP = \frac{Gained\ thermal\ energy\ from\ PVT}{Energy\ consumption\ of\ fan} \tag{22}$$

To determine the mass transfer rate, the mass transfer coefficient, which can be calculated with the Biot number (Bi) is, used [2]:

$$Bi = \frac{h_m L}{D_e} \tag{23}$$

The Bi is dimensionless and it means a criterion, which gives a direct indication of the relative importance of conduction and convection in determining the temperature history of a body being heated or cooled by convection at its surface. D_e is the effective diffusivity coefficient.

In other formulation between two dimensionless numbers, the Dinçer number (Di) is used to determine the Bi [35]:

$$Bi = \frac{24.85}{Di^{0.375}} \tag{24}$$

Di, which states the effect of the drying air velocity on the product drying coefficient, can be implemented in the drying process [36]:

$$Di = \frac{V}{k_c L} \tag{25}$$

Di expresses the relationship between the property of the fluid medium and the heating or cooling rate of the solid object. In other words, it defines the effect of fluid property on the thermal parameter of the solid object with regular or irregular shapes. k_c is the drying constant.

The drying constant (k_c) can be calculated with the following equation [36]:

$$\text{-}k_c(M_t\text{-}M_e) = \frac{dx}{dt} \tag{26}$$

In experimental studies, the uncertainty arising from measurements or measuring devices must be determined. R is the quantity to be measured, the independent variables affecting the R quantity are expressed as x_1, x_2, x_3, …, x_n, and the error rates of each independent variable are expressed as w_1, w_2, w_3, …, w_n. Uncertainty analysis (W_R) can be computed with the following equation [37]:

$$W_R = \left[\left(\frac{\delta R}{\partial x_1}w_1\right)^2 + \left(\frac{\delta R}{\partial x_2}w_2\right)^2 + \ldots + \left(\frac{\delta R}{\partial x_n}w_n\right)^2\right]^{1/2} \tag{27}$$

Uncertainty analysis is a powerful method for experimental studies

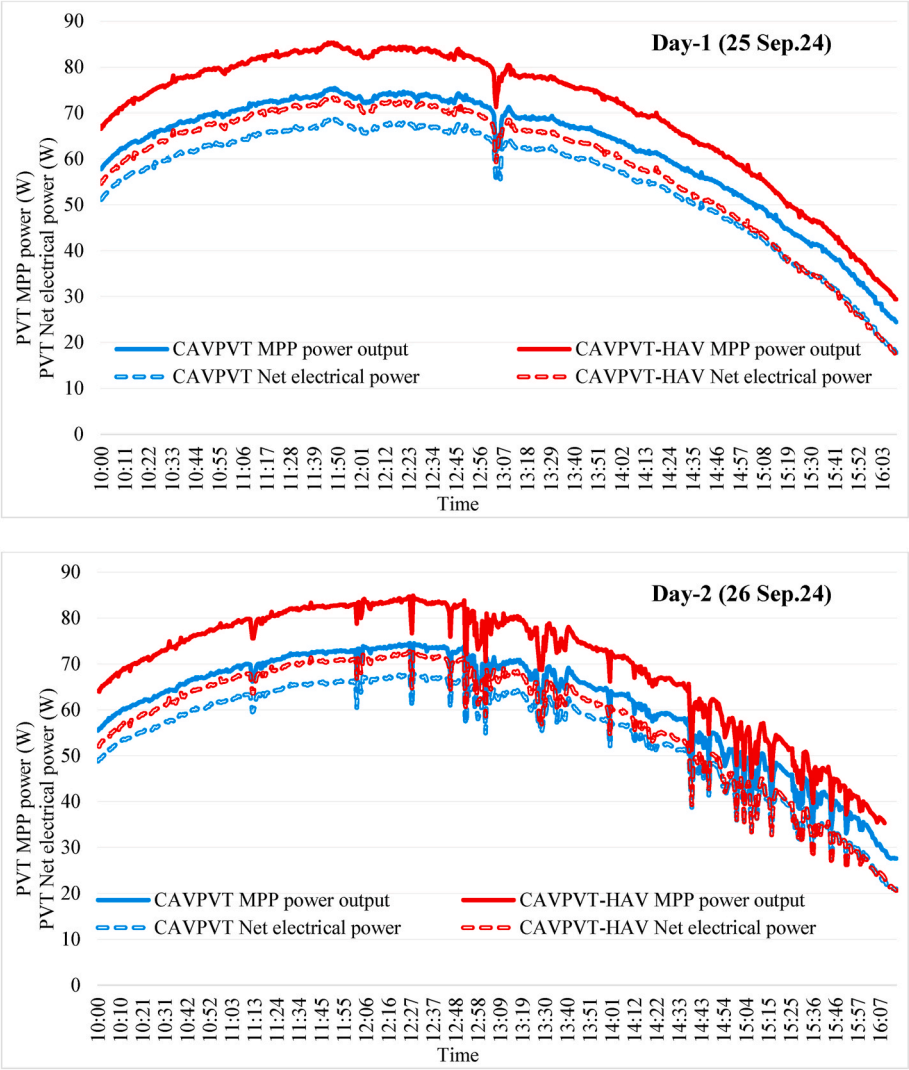

Fig. 10. Instantaneous variation at the MPP power output and net electrical power of PVTs.

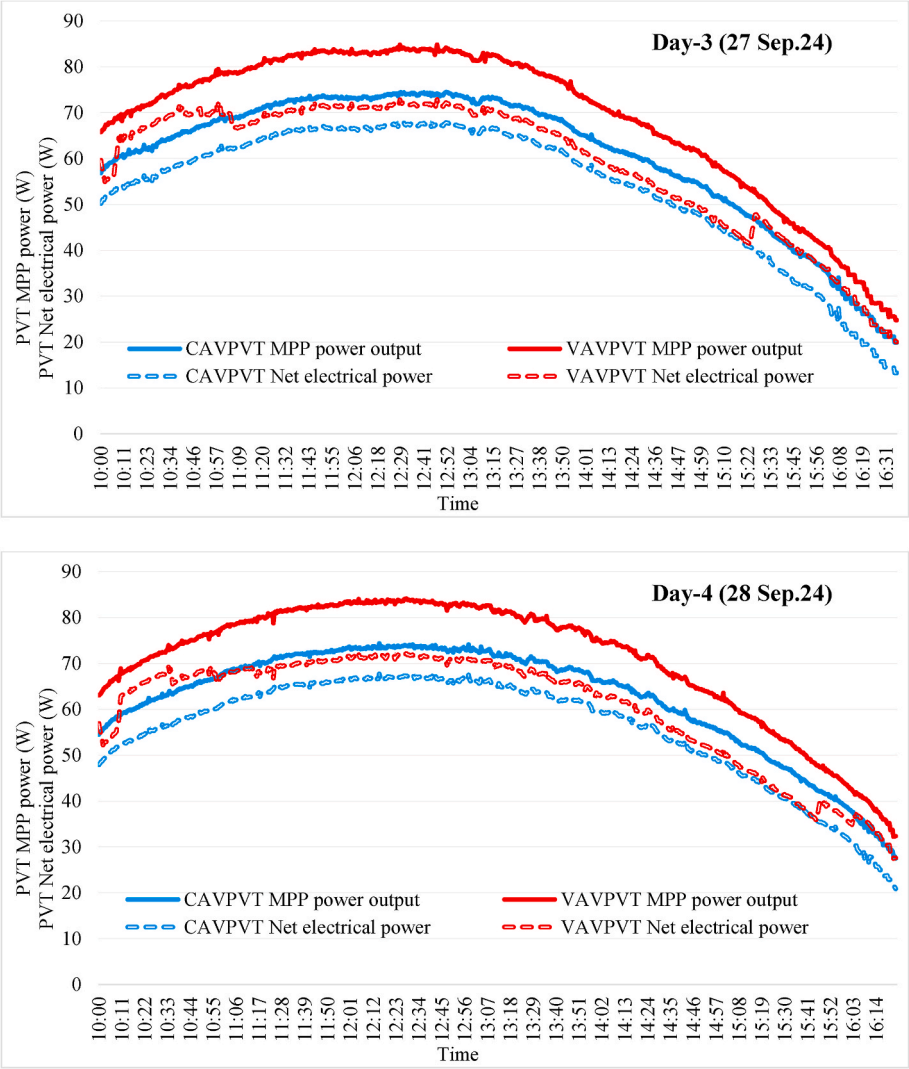

Fig. 10. (*continued*).

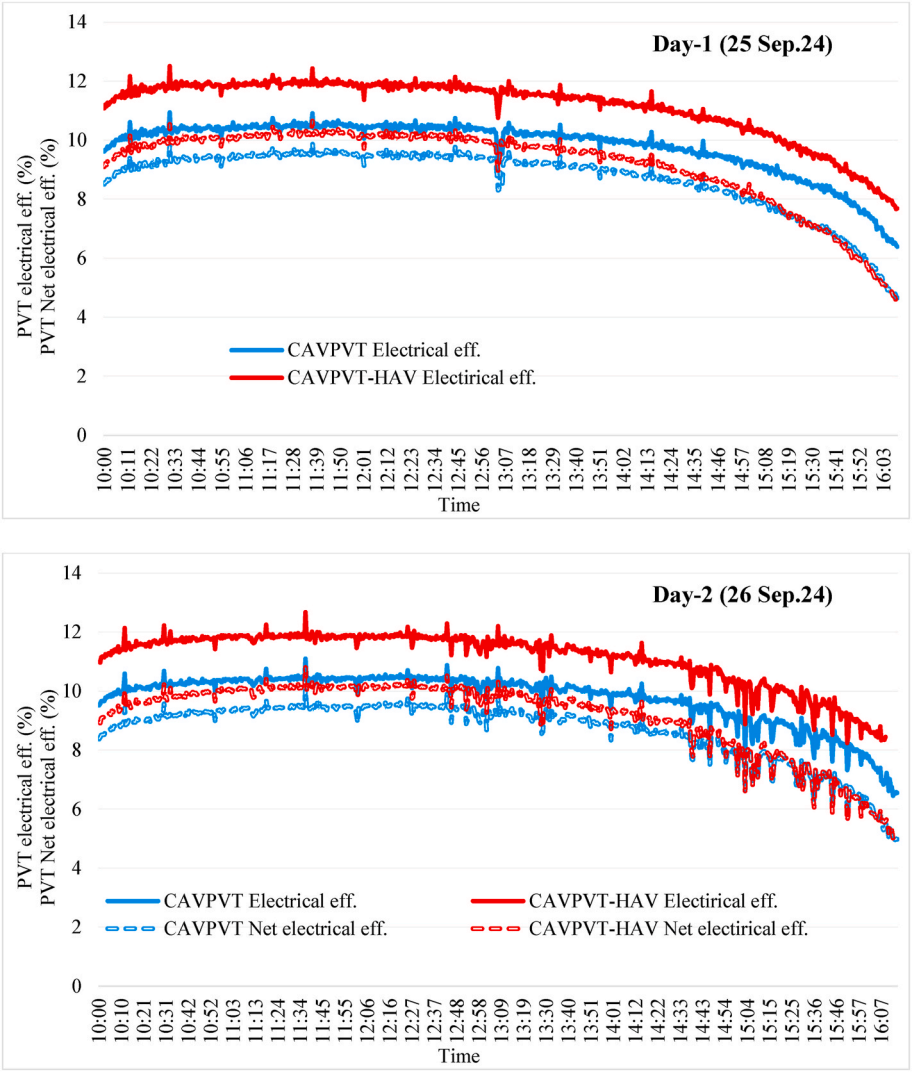

Fig. 11. Variation of instantaneous electrical efficiency at the PVT and net electrical efficiency.

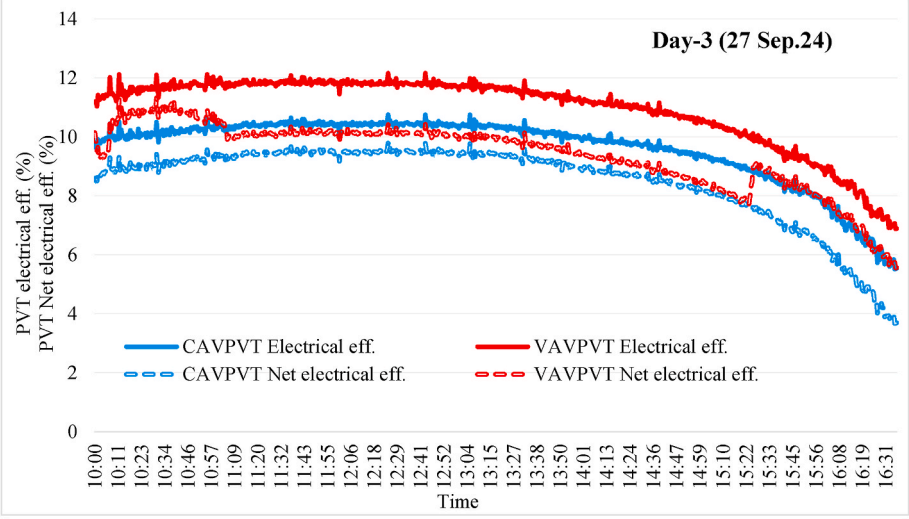

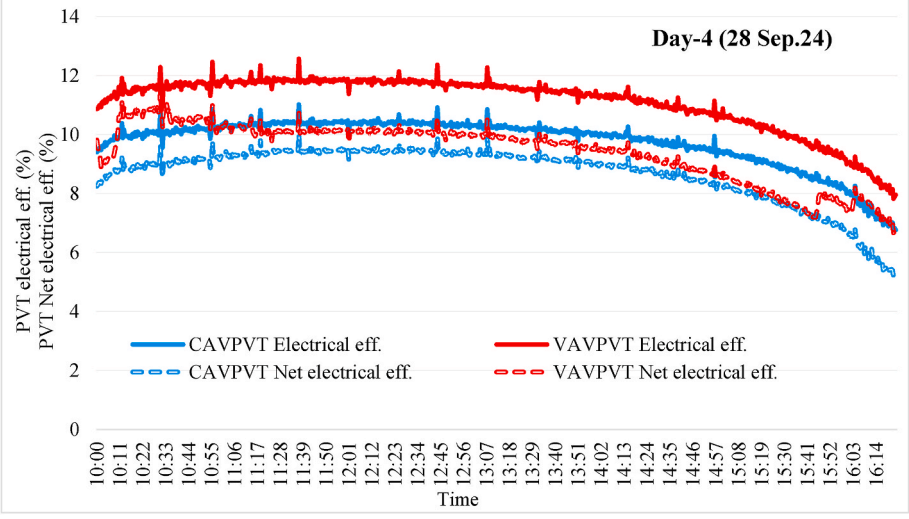

Fig. 11. (*continued*).

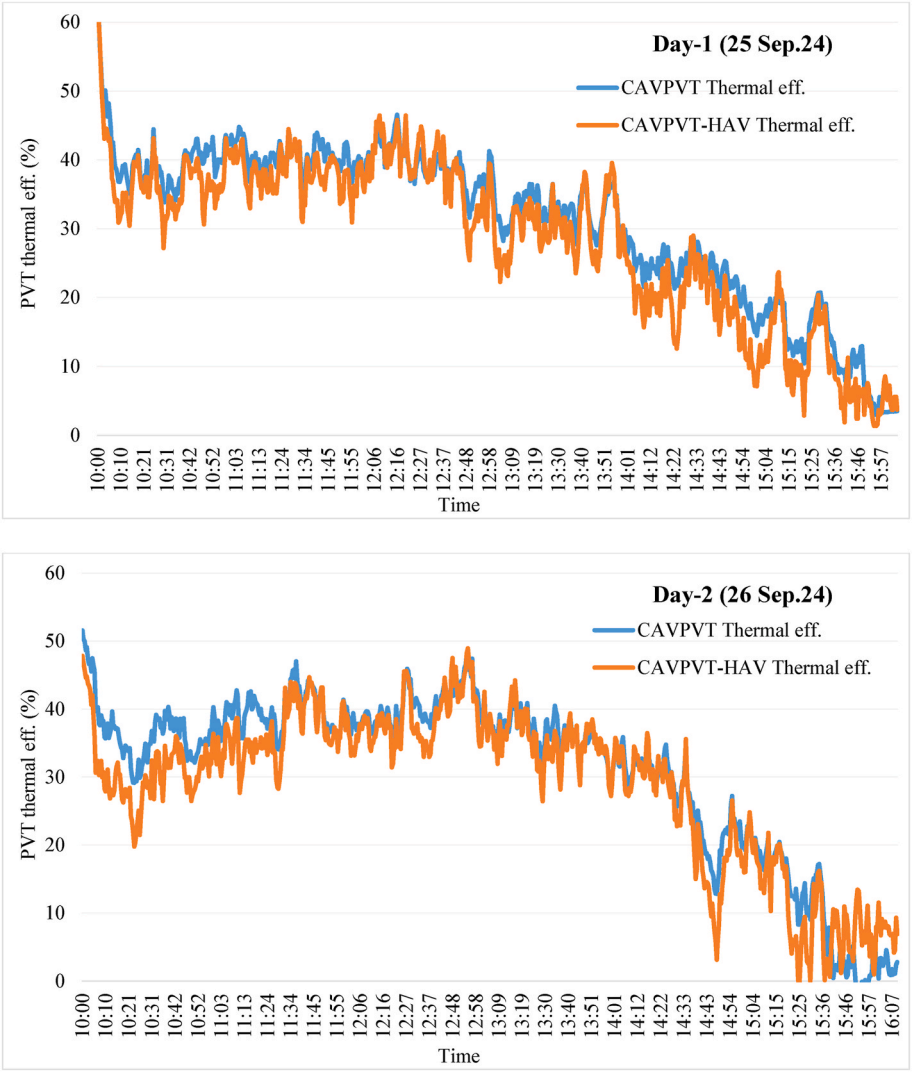

Fig. 12. The variation of instantaneous thermal efficiency at the PVT in experiments.

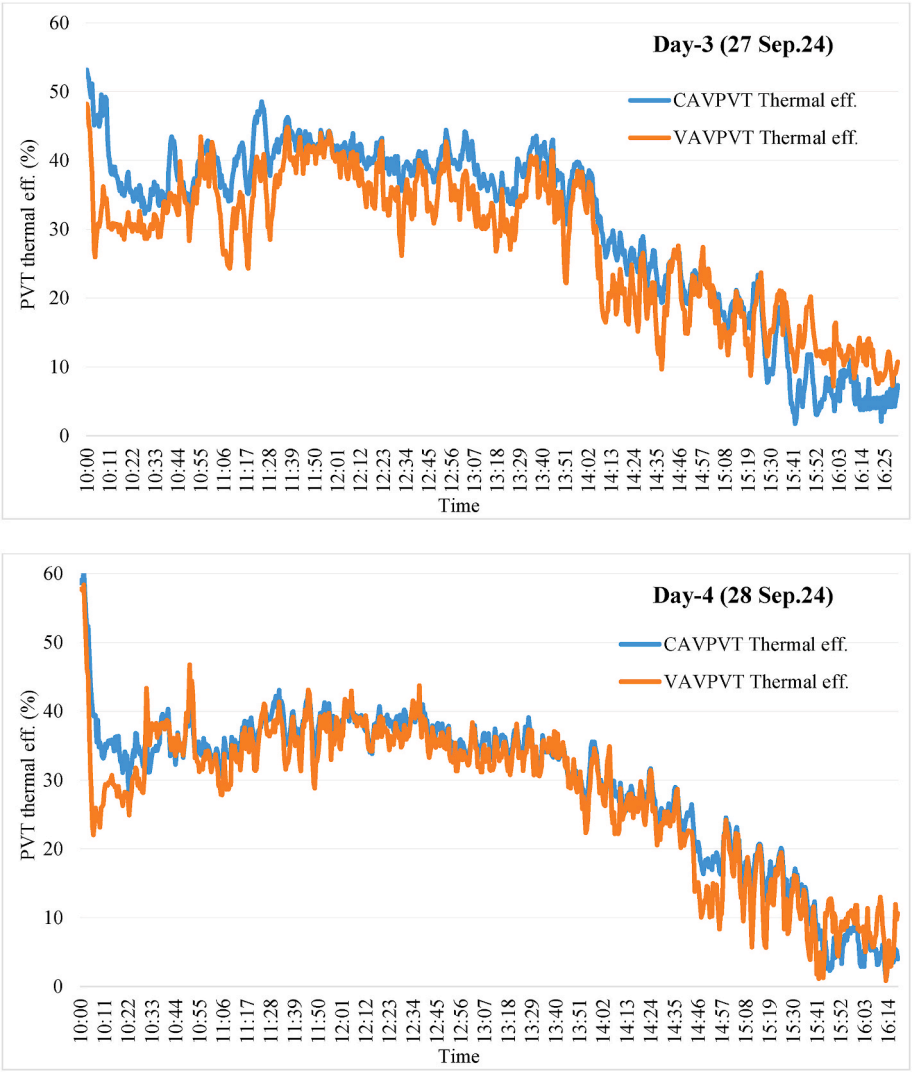

Fig. 12. (*continued*).

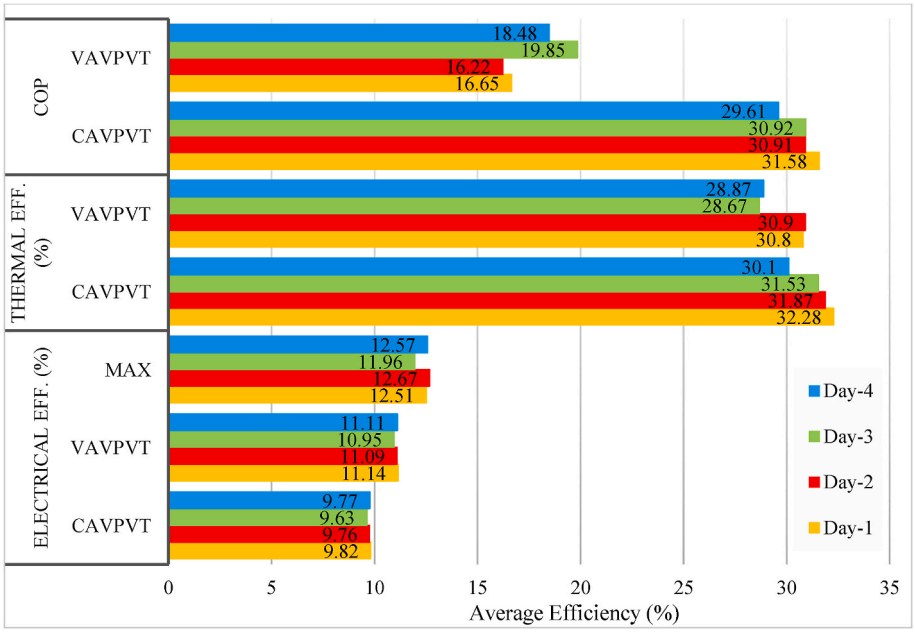

Fig. 13. Comparison of thermal efficiency, electrical efficiency, and COP.

and is performed using Eq. (27). In the uncertainty analysis, reading errors, errors originating from the connection element structure—connection points, and errors originating from the measurement device accuracy affect the calculated error value. The uncertainty values were calculated as ±6.455 W/m^2 for solar radiation, ±0.141 % for temperature measurement, ±2.415 % for relative humidity measurement, ±3.241 % for PV electrical power, ±1.114 % for PV thermal power, ±1.242 % for COP value, ±0.026 m/s for air velocity measurement, and ±0.024 g for dried product mass measurement. It has been observed that the variables or values within the scope of the study whose uncertainty values were calculated are acceptable in terms of the measurement technique.

The exergy input ($E_{x,in}, W$) and exergy output ($\dot{E}_{x,out}, W$) derived from solar energy can be expressed as follows:

$$\dot{E}_{x,in} = AS_{irr}\left[1-\frac{4}{3}\left(\frac{T_a}{T_s}\right)+\frac{1}{3}\left(\frac{T_a}{T_s}\right)^4\right] \tag{28}$$

$$\dot{E}_{x,out} = \dot{Q}_{loss}\left(1-\frac{T_a}{T_{cell}}\right) \tag{29}$$

In Eq., T_s (K) represents the temperature of the sun (5770 K), while T_{cell} (K) denotes the temperature of the PVT collector's cell. Additionally, $\dot{Q}_{loss}$ (W) refers to the heat loss. The exergy balance equations are provided in the following expressions [21]:

$$\sum \dot{E}_{x,d} = \sum E_{x,in} - \sum E_{x,out} \tag{30}$$

$$\sum \dot{E}_{x,d} = \sum E_{x,in} - \sum \left(E_{x,th} + E_{x,PV}\right) \tag{31}$$

$$\dot{E}_{x,th} = \dot{Q}_u\left(1-\frac{T_{amb}}{T_{out}}\right) \tag{32}$$

$$\dot{E}_{x,PV} = \eta_{el}AG\left[1-\frac{4}{3}\left(\frac{T_{amb}}{T_s}\right)+\frac{1}{3}\left(\frac{T_{amb}}{T_s}\right)^4\right] \tag{33}$$

$$\dot{E}_{x,PVT} = E_{x,th} + E_{x,PV} \tag{34}$$

$\dot{E}_{x,d}$ (W) represents the exergy destruction, while the exergy efficiency of the PVT collector is given in Ref. [21]:

$$\eta_{ex} = 1-\frac{\dot{E}_{x,d}}{\dot{E}_{in}} = \frac{\dot{E}_{x,out}}{\dot{E}_{x,in}} \tag{35}$$

The annual amount of energy produced by the PVT system was calculated by taking an average of 7.5 h of solar irradiance per day. Electricity and natural gas prices were accepted as 0.15 $/kWh and 0.343 $/m^3.

Since the two systems are identical in all calculations, the extra amount spent for CAVPVT is calculated as $15. The annual amount of electricity and heat produced in CAVPVTD and VAVPVTD systems is calculated using the equations. The payback period of CAVPVTD compared to VAVPVTD is calculated based on the difference in the average electricity and heat produced by CAVPVTD and VAVPVTD systems. The following formula is used to compute annual cost (AC):

$$AC_1 = W \times N \times ET \tag{36}$$

$$AC_2 = M_{gas} \times N \times NT \tag{37}$$

In Eqs., W is the power consumption, N is the daily working time in a year, and ET and NT are the unit prices of electricity and natural gas. The payback period (PP) of the PVT system is defined as the ratio between the total investment cost (TIC, $) and AC_{total} ($AC_1 + AC_2$, $/year) and is expressed as follows [21]:

$$PP = TIC/AC_{total} \tag{38}$$

4. Findings and discussion

This study involves testing over four days. On the first and second days, tests are carried out at constant air volume. One of the systems is run at constant air velocity on the third and fourth days of operation. On the other hand, the other is run with varying air volume based on the temperature of the PV surface. Thus, the effects of air velocity and temperature were observed on four different days. Some abbreviations are used in the following sections, these are; CAVPVTD, CAVPVTD-HAV, and VAVPVTD, as shown in Table 1.

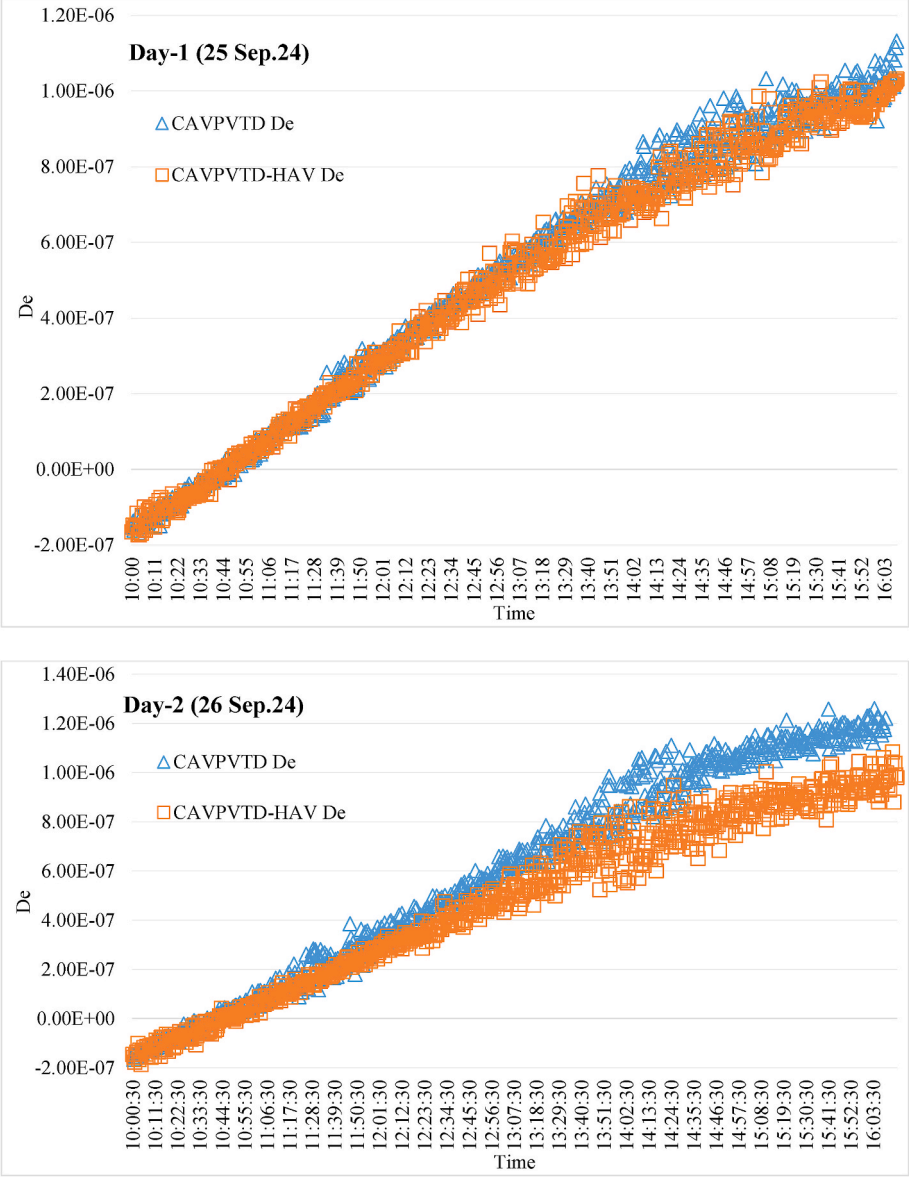

Fig. 14. The variation of instantaneous *De* over time.

4.1. Electrical and thermal analyses

The experiments were performed over four consecutive days (25–28 September) to test the electrical and thermal performance of two systems with the same features under different conditions. The changes in environmental factors during the trials, including relative humidity, ambient air temperature, and sun radiation, are illustrated in Fig. 6. Although fluctuations were observed due to cloudiness on the second day, solar irradiation values formed similar curves in all experiments. The average solar irradiation values on Days 1, 2, 3, and 4 were 968.35 W/m^2, 956.96 W/m^2, 957.05 W/m^2, and 976.56 W/m^2. The average ambient air temperatures were measured as 28.19 °C, 28.77 °C, 29.73 °C, and 31.76 °C for each of the four cases.

Fig. 7 shows instantaneous variation in outlet air temperatures (OATs) and surface temperatures for CAVPVTD, CAVPVTD-HAV, and VAVPVTD. On the first day and second day, it was observed that OATs in CAVPVTD and CAVPVTD-HAV systems had similar curves. While there was a significant difference between OATs due to solar irradiation in most of the experiments, close values were observed towards the end of the day. The average OAT of CAVPVTD was 4.2 % higher than the other on the first day. This difference was measured as 4.06 % on the second day. In the system with high air velocity (CAVPVTD-HAV), OAT values are mostly lower than the other, which means that drying is done at low temperatures. Accordingly, it can be said that the drying rate is low and the drying time is extended. Although it was observed that the OATs in the CAVPVTD and VAVPVTD systems had similar curves on the third and fourth days, at the end of the third-day experiment, the OAT curve of CAVPVTD cut the OAT curve of VAVPVTD and reached lower temperatures. The average OAT of CAVPVTD was 2.85 % higher than the other on the third day. This difference was obtained as 2.64 % on the fourth day. On the third and fourth day, it was observed that the OATs in the CAVPVTD and VAVPVTD systems had similar curves, but at the end of the third day of the experiment, the OAT curve of the CAVPVTD intersected the OAT curve of the VAVPVTD and reached lower temperatures. This is because, while the fan speed in the CAVPVTD was constant throughout the day, In the VAVPVTD system, the fan, which operates depending on the PV temperature set at 40 °C, reduced its speed towards the end of the day and lowered the variable air volume

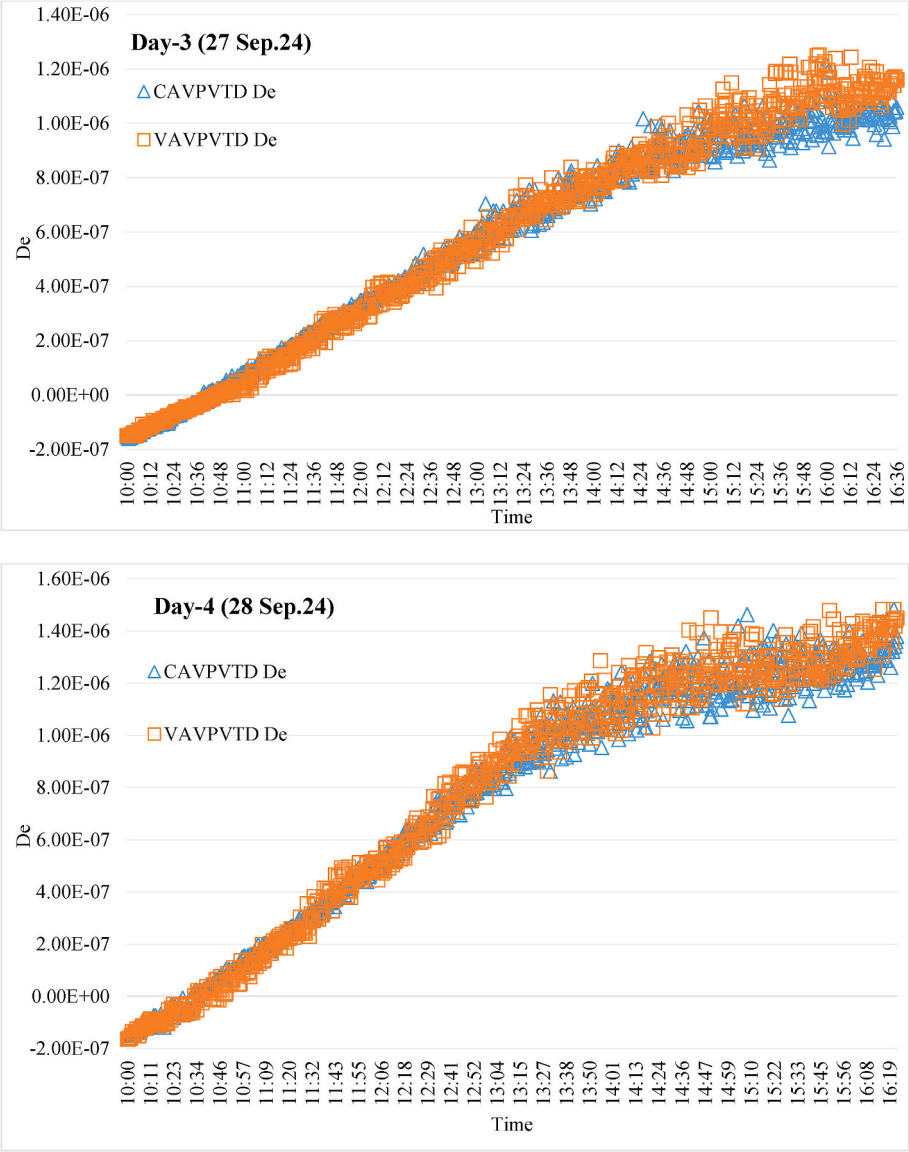

Fig. 14. (*continued*).

value. This reduced the OAT values of the VAVPVTD. In this case, it also positively affected the drying rate. In all experiments, the surface temperatures of PVT in CAVPVTD-HAV were always lower than those of PVT in CAVPVT. On the first day, the average surface temperature of PVT in CAVPVTD was 5.76 % higher than the CAVPVTD-HAV. This difference was measured as 5.63 %, 7.15 %, and 4.26 % on the Day-2, Day-3 and Day-4, respectively. This means that it provides good cooling due to the high variable air volume value. Of course, sometimes the variable air volume values were lower than the constant air volume one (Day-2 and Day-3) but still, it managed to keep the surface temperature lower. Thus, a higher electrical efficiency was achieved.

Temperature and humidity parameters were selected as the inputs of the control algorithm. Fan speed was determined as the output parameter. In the systems, all sensor values were measured at 1-min intervals and 10 ms intervals during each reading, and 10 data points were averaged. Thus, the average value method was used to prevent erroneous measurements. This method was used to see the effect experimentally. On the other hand, long-term data can be filtered, a smoother measurement can be made, and a more precise control method can be made. In addition, the fan motor speed was controlled in 10 different speed ranges, and more precise flow ranges can be obtained by increasing this range. Fig. 8 shows the instantaneous variation of air velocity. While the inlet air velocity is constant in CAVPVTD, the air velocity is constant in CAVPVTD-HAV but higher than the other. In VAVPVTD, the inlet air velocity is variable, velocity control was provided by the algorithm prepared depending on the external weather conditions and, therefore, the PV surface temperature. In instances when the prepared algorithm offered speed control, it operated the fans at maximum speed to dissipate the heat energy that had gathered at the start of the experiment. This caused the product with high product humidity to dry faster. Then, the algorithm reduced the speed of the fans and stayed there for a while. Then, it increased to maximum speed again depending on the PV surface temperature and stayed there for a long time. Finally, towards the end of the experiment, the fan speed decreased again as the solar irradiance decreased. With the decrease in fan speed at the end of the experiment, the drying rate also increased considerably.

Fig. 9 shows the images of the thermal camera taken on the fourth day. The one on the right shows the thermal images of the moment when it is used with constant air volume, and the one on the left shows the moment when it is used with variable air volume. It is evident how the fans are cooling the area. In general, in air cooling applications of PVTs,

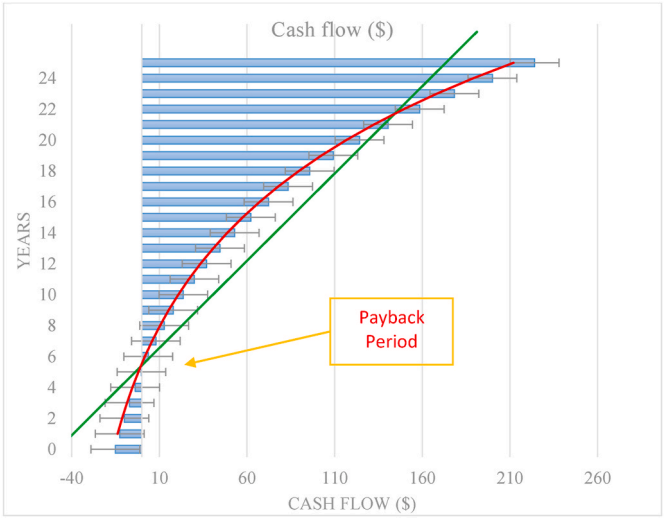

Fig. 15. The VAVPVTD's 25-year depreciation graph (Bar: Cash flow, Red line: 2 per Mov. Avg., Green line: Linear regression and I: Standard error). (For interpretation of the references to color in this figure legend, the reader is referred to the Web version of this article.)

the hottest areas are the upper (air outlet) areas of the PVT, while in this design, it has been observed that a large part of the PVT is cooled and the lower center (air inlet) areas are hotter. Although this design shows that it provides good cooling, it does not provide equal cooling and it has been revealed that the hole diameters should be gradually reduced instead of the fixed hole diameter in the air direction and channels in the PVT structure.

Maximum Power Point (MPP) can be used to assess the maximum electrical power transfer generated by the suggested PVTs to the load. Solar irradiance, ambient temperature, and solar cell temperature are just a few of the variables that affect PVTs' MPP. Fig. 10 illustrates the instantaneous variation in the MPP power output and net electrical power of PVTs. Although similar curves were generally observed, fluctuations were observed depending on solar irradiation in the second day experiment. The highest instantaneous PVT MPP was achieved as 85.34 W on the first day and in CAVPVTD-HAV. This can be attributed to the better cooling due to the higher air velocity in CAVPVTD-HAV. Net electrical power means subtracting the power consumed by the fan from the power produced by the PVT. The instantaneous variation in net electrical power curves in CAVPVTD moved parallel to the MPP power output curves in all experiments. Although the instantaneous change curves in the net electrical power in VAVPVTD moved parallel to the MPP power output curves in the first two experiments, they showed differences from time to time in the last two experiments, especially at

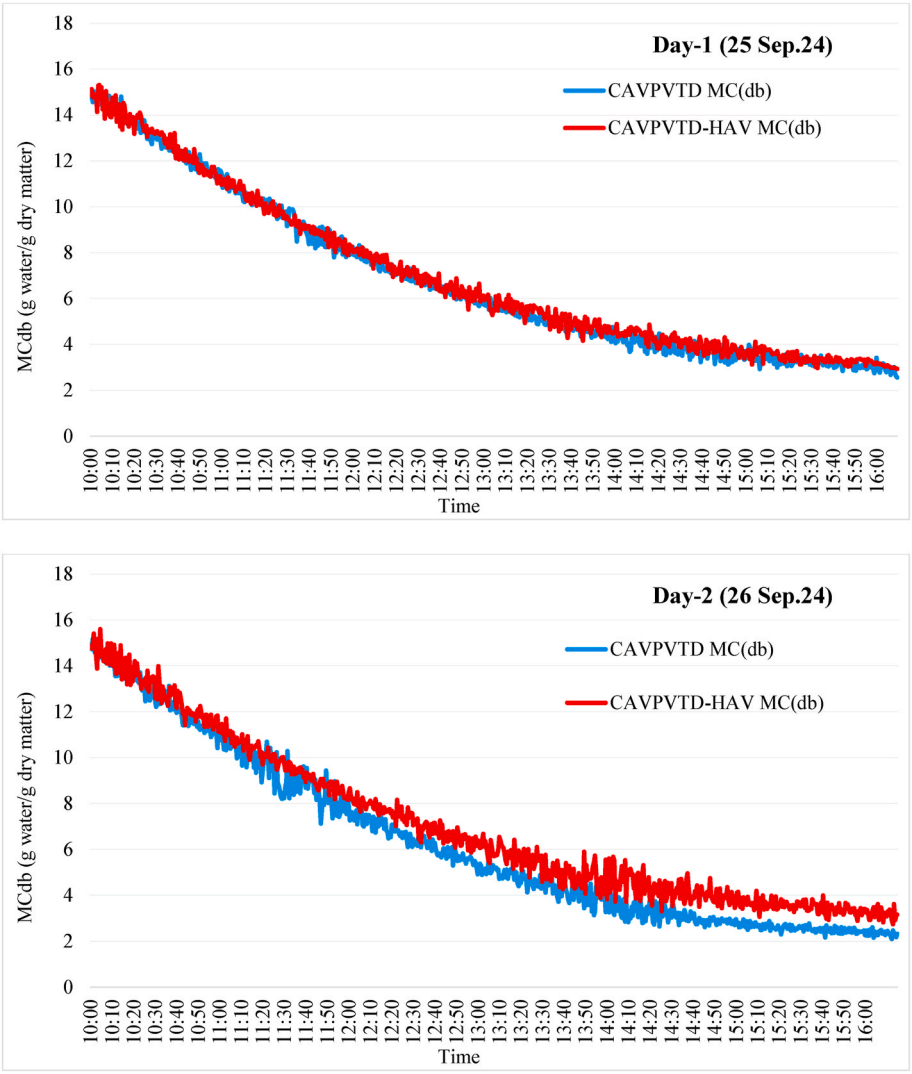

Fig. 16. The variation of instantaneous moisture content.

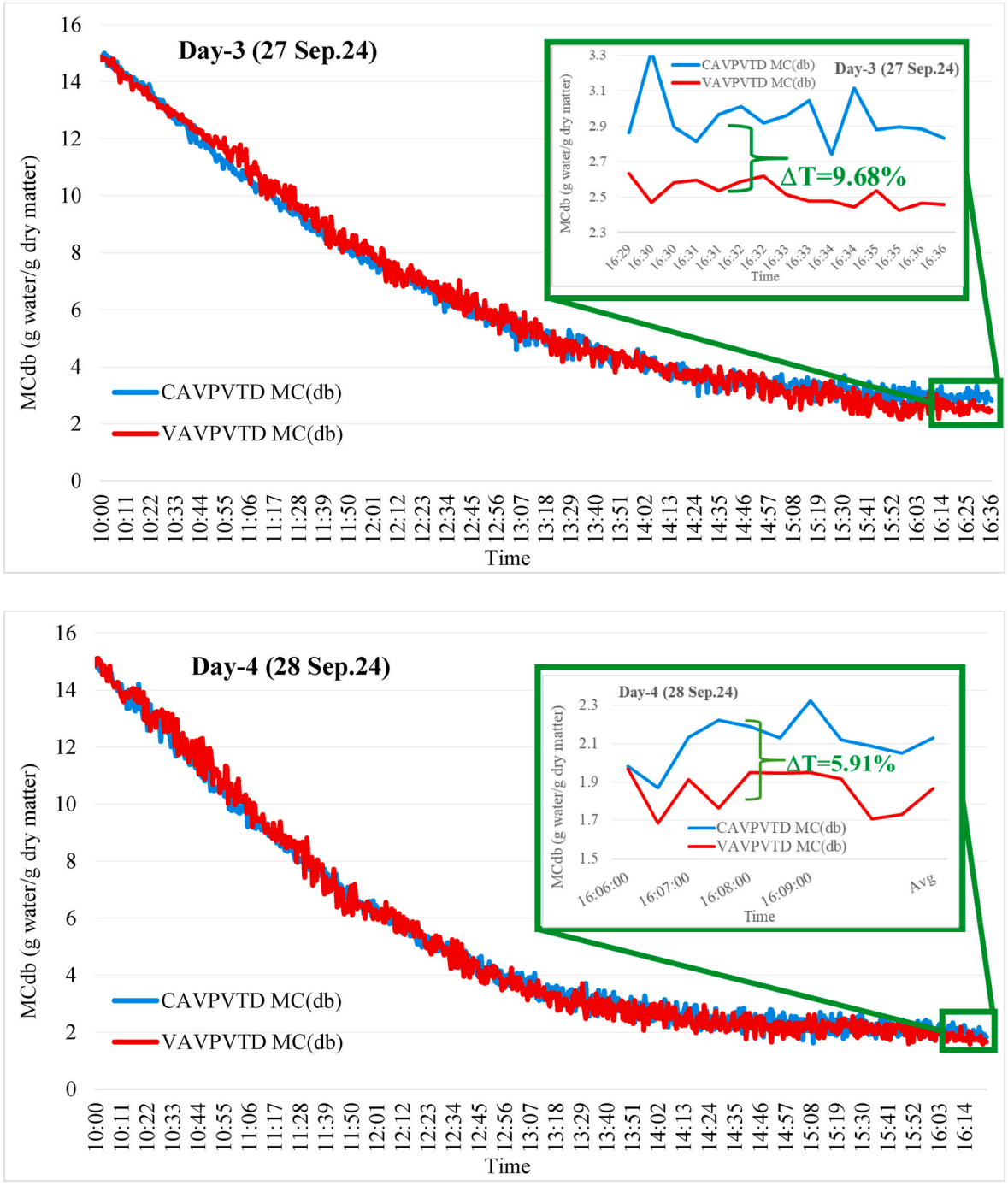

Fig. 16. (*continued*).

the beginning and end of the experiment, depending on the power consumption of the fan. This situation is due to the fan increasing its speed to keep the system at the desired value, and therefore, the power consumption of the fan increases. Average net electrical powers are lower by 5.59 %, 5.53 %, 9.6 %, and 8.29 % on a day-by-day basis, respectively, compared to MPP power output, indicating lower fan energy consumption in the first two experiments.

Fig. 11 shows how instantaneous electrical and net electrical efficiencies vary during tests. The maximum electrical efficiency was 12.67 % on the second day in CAVPVTD-HAV, but the values obtained on the other days were also quite close to this value. The maximum electrical efficiency was found to be 12.51 %, 11.96 %, and 12.57 % on days 1, 3 and 4, respectively. On the other hand, when the average electrical efficiencies were compared, the highest was 11.14 % on the first day in CAVPVTD-HAV. It was obtained as 11.11 %, 11.09 %, and 10.95 % on days 4, 2 and 3, respectively. This means an increase in electrical efficiency of up to 13.79 %. [4], and amorphous silicon PV, which was 5.7 % [6]. They obtained different results depending on the PV panel used, the method, and the weather conditions. Comparable findings were observed for glass-to-glass type PV, which was 12.44–14.06 % [8], and monocrystalline PV, which was 13.49 %. Studies on PVT have generally focused on the electrical efficiency of the PVT [4,6,8]. The fan's usage is taken into consideration when calculating net electrical efficiency. Accordingly, as expected, net electrical efficiency is lower in all experiments compared to electrical efficiency based solely on electricity production. Based on average net electrical efficiency, the highest net

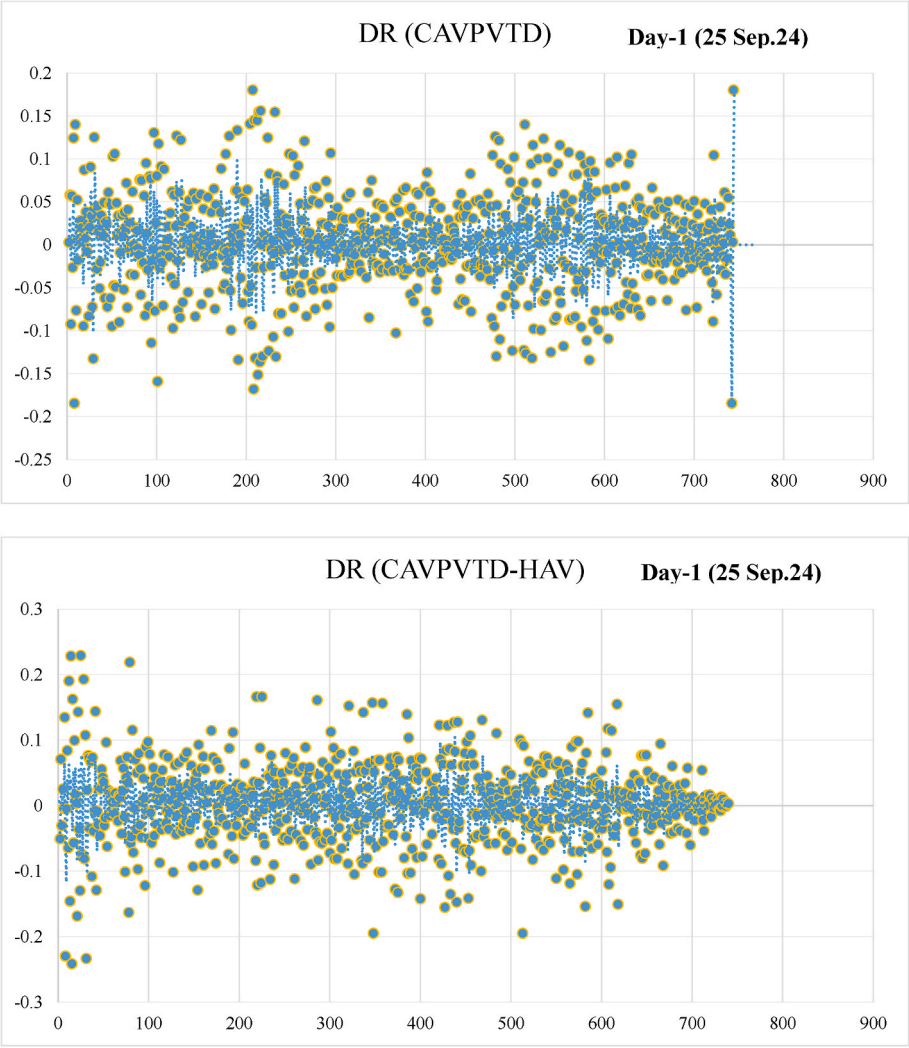

Fig. 17. The variation of instantaneous DR with time.

electrical efficiency is 9.4 % and 9.44 % in VAVPVT on Day-3 and Day-4, respectively. Based on electrical efficiency and net electrical efficiency, each experiment is compared among themselves and the highest difference is in Day-3 with 10.37 %. On the other hand, the lowest difference is in Day-1 and Day-2 which are very close to each other. As a result, although there are serious decreases in net electrical efficiency on Day-3 and Day-4 due to the fan, it is seen that the highest efficiency is again in VAVPVT on Day-3 and Day-4. This situation indicates the advantage of using variable velocity.

The variation in instantaneous thermal efficiency at the PVT during the trials is displayed in Fig. 12. Although VAV control significantly increases the electrical efficiency in PVT, the thermal efficiency was lower compared to CAVPVT. On the other hand, it was observed that the thermal efficiency increases as the air temperature increases, as in Day-4. When comparing average thermal efficiencies on Day-1, Day-2, and Day-4, CAVPVT outperformed CAVPVT-HAV by 6.8 %, 5.61 %, and 4.09 %, respectively. When comparing average thermal efficiencies, the highest value was 32.28 % in CAVPVT on Day-4, while the lowest value (28.67 %) was in VAVPVT on the same day. The average thermal efficiency was determined by Arslan and Aktaş [4] and Kong et al. [6] to be 43.75 % and 46.8 %, respectively, while the maximum thermal efficiency was reported by Gupta et al. [8] to be 36.01 %. On Day-3, interestingly, CAVPVT showed a significant performance superiority over CAVPVT-HAV by 26.34 %. This may be because VAVPVT operated at a much lower air volume than CAVPVT for one-third of the experimental period and at a higher air volume for two-thirds of it. Furthermore, it is hypothesized that this might be caused by the high PVT surface temperature that persists throughout the day. This illustrates the air velocity's effectiveness in terms of thermal efficiency. It can be said that thermal efficiency increases as air temperature increases and air velocity decreases.

Fig. 13 compares thermal efficiency, electrical efficiency, and COP. In the VAV-controlled system, the algorithm mostly increased the fan power consumption to the maximum values due to the high outdoor air temperature and surface temperature, so the COP value was always lower than the constant air volume. In terms of COP, it is thought that the air volume value set in the CAV system may be optimum. When the systems were evaluated in terms of thermal efficiency, the CAVPVTD system performed better than the other with a small difference. This is due to the higher air speed in the VAV system. When the systems were evaluated in terms of electrical efficiency, the VAVPVTD system performed better than the other with a small difference. For the tested systems and conditions, it was determined that the VAVPVDTD performed well in terms of electrical efficiency, but slightly lower in terms of thermal efficiency and significantly lower in terms of COP. The electrical, thermal, and drying performance of the system, known as the total (integrated) system performance, is affected by the system design parameter and operating conditions. Therefore, ranges of parameters

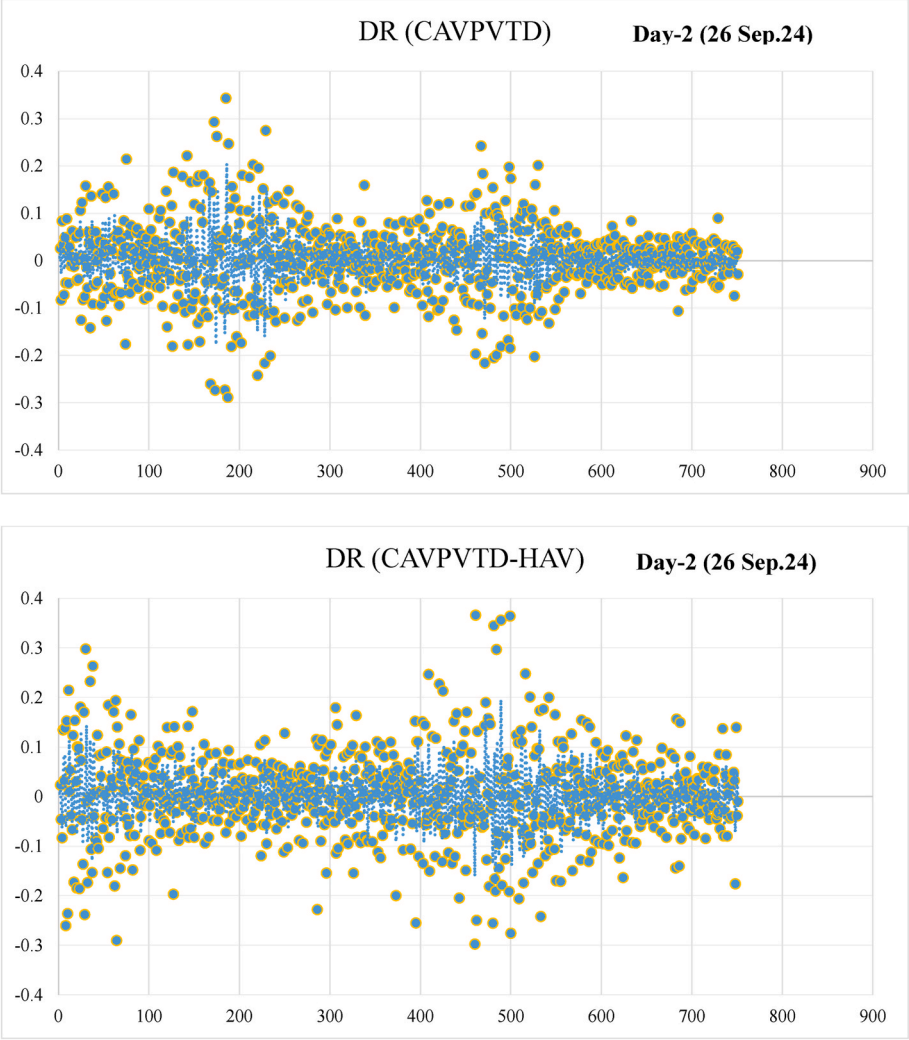

Fig. 17. (*continued*).

were employed in the trials. VAV control and innovative design applications reduced drying time and boosted electricity efficiency by up to 12.06 %. Conversely, PVT performed worse in terms of thermal efficiency, reaching 9.9 %. Additionally, VAVPVTD had a drying effectiveness improvement of up to 10 %. The best result in terms of net electrical power was achieved on Day-4 in VAVPVT Net electrical power. On the other hand, the highest difference in VAVPVT net electrical power compared to that of CAVPVT was on Day-3 with 8.76 %. The increase in drying air temperature and airflow rate increased the heat transfer in the product, which positively affected the drying performance by increasing the drying rate of the apple slices.

The mass transfer coefficients in trials ranged from 1.14 × 10−3 m/s to 4.1 x 10−6 m/s. Fig. 14 shows the instantaneous De variation over time. As can be seen from the graphs, while similar values were generally formed in other experiments, a separation was observed towards the end of the experiment on Day-2. It is thought that this situation is due to the effective air volume. When comparing the average effective diffusivity coefficients, they varied between 4.8 × 10−7 m^2/s and 7.75 × 10−7 m^2/s. The highest value was obtained in VAVPVTD on Day-4. CAVPVT was superior by 4.4 % and 20.38 % on Day-1 and Day-2, respectively, but was less successful with a lower De value of 2.31 % and 2.2 % on Day-3 and Day-4, respectively. It was observed that De increased with increasing drying air temperature consistent with previous researchers [7,8]. Fterich et al. [7] reported that De was 1.02 × 10−9 m^2/s and 3.27 × 10−9 m^2/s for tomatoes at drying air temperatures of 40 °C and 60 °C, respectively. Gupta et al. [8] obtained 4.97 × 10−9 m^2/s for green tea drying in mixed-mode drying.

4.2. Exergy analysis

On Day-1, the efficiency of the CAVPVT system was calculated as 23.67 %, while the efficiency of the VAVPVT system was 25.32 %; on Day-2, CAVPVT efficiency was 22.89 %, VAVPVT efficiency was 24.56 %; on Day-3, CAVPVT efficiency was 22.49 %, VAVPVT efficiency was 26.13 %; and on Day-2, CAVPVT efficiency was 24.08 %, VAVPVT efficiency was 28.16 %. The overall average of the CAVPVT system was 23.28 %, while the VAVPVT system was 26.04 %. When the experimental results were examined, it was clearly seen that the CAVPVT system provided higher exergy efficiency than the VAVPVT system in all four experiments. The fact that the VAVPVT system exhibited higher efficiencies compared to the CAVPVT system showed that this system experienced less loss in energy conversion and provided more efficient energy production. In particular, the efficiency of the VAVPVT system on Day-3 is the highest value at 26.13 %, which shows that the VAVPVT can reach maximum performance under certain conditions. These data show that the VAVPVT system offers a higher exergy efficiency compared to the CAVPVT system in general, and therefore the energy conversion is more efficient. The average exergy efficiency of the VAVPVT system is calculated as 26.04 %, while the average of the CAVPVT system is 23.28 %. This difference shows that the VAVPVT

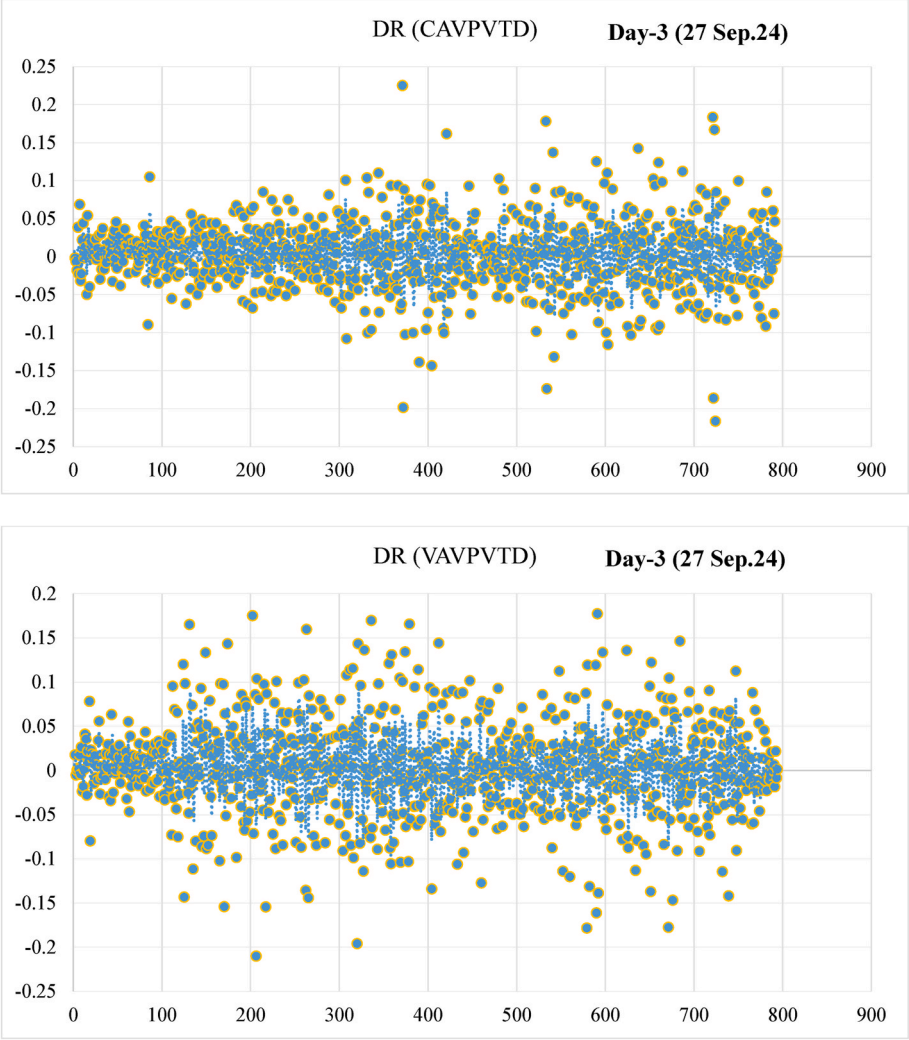

Fig. 17. (*continued*).

system provides higher-quality energy production and can transfer more work to its environment. This superior performance of the VAVPVT system offers a great advantage, especially in terms of energy efficiency and sustainability. A system with high exergy efficiency provides more benefits with less energy loss, which shows that the system is more efficient in economic terms. This situation shows that the VAVPVT system has the potential to produce more energy while creating a lower environmental impact. As a result, it is understood that the VAVPVT system stands out in both aspects (energy efficiency and environmental sustainability) and provides a more efficient energy conversion process. These data show that the VAVPVT system offers an ideal solution, especially for projects targeting higher efficiency and lower energy loss, and can provide longer-term economic benefits in energy production.

4.3. Economic analysis

The CAVPVT system's 25-year depreciation curve in comparison to the VAVPVT system is displayed in Fig. 15. The difference in electrical and heat power from all four experiments is averaged to determine the payback period of the additional $15 investment in the CAVPVT system. Fig. 15 illustrates that the suggested CAVPVT system has a 5.05-year payback period. The system is predicted to start making exponential profits during the fifth year of operation. Consequently, the system design is both sustainable and effective.

4.4. Drying characteristics

Daily variations in drying air temperatures and relative humidity influenced both the drying rate and the duration of the drying process. On Day-1, the maximum drying chamber outlet air temperature (MDCOAT) in CAVPVTD-HAV was 1.62 % greater than that in CAVPVTD. The MDCOATs for the other days were found to be 1.53 %, 2.74 %, and 1.64 % higher, respectively. As expected, the maximum drying chamber outlet temperature was 38.93 °C and 39.57 °C on Day 4, CAVPVTD and VAVPVTD, respectively. With the effect of temperature, drying rates increased and drying time was accordingly shortened. These findings highlight the importance of temperature control and air velocity for optimizing drying processes. On Day-1, the average drying chamber outlet air relative humidity (ADCARH) in CAVPVTD-HAV was 2.34 % greater than that in CAVPVTD. The ADCARHs for the other days were found to be 0.48 %, 7.98 %, and 2.69 % higher in the variable air volume system, respectively. Accordingly, the highest ADCARH occurred in VAVPVTD on Day-3. This showed that it was effective in reaching a lower final moisture content value (9.68 %) compared to the other system.

The drying characteristics of apple slices were presented concerning moisture behavior as a function of time. Experimental data on the drying of apple slices was collected by experimentation to determine the aptness of the algorithm. Fig. 16 shows graphically the effect of drying air temperature on moisture content in apple slices. The initial moisture

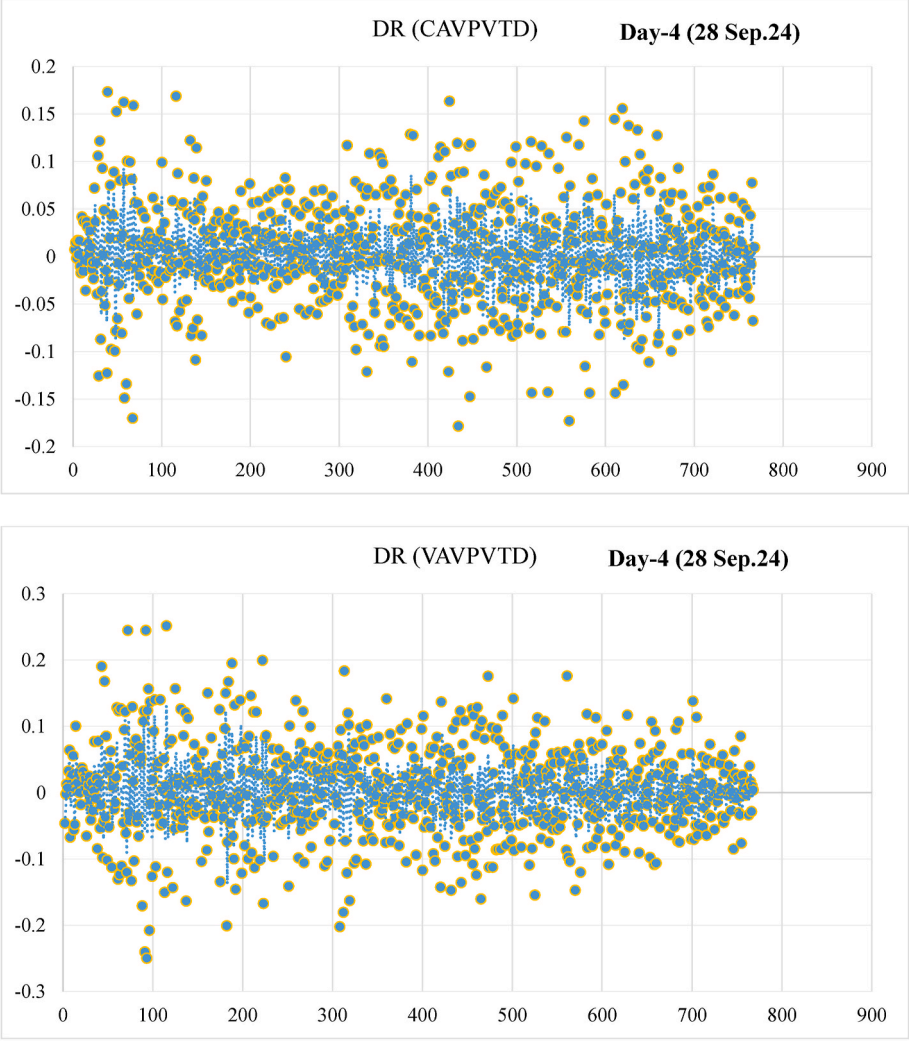

Fig. 17. (*continued*).

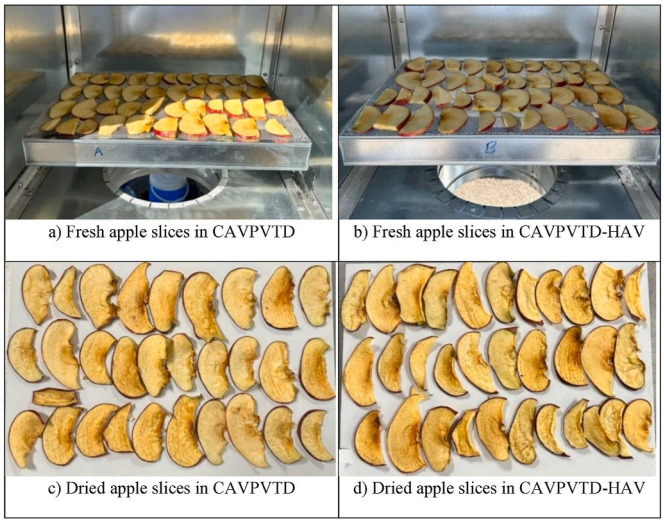

Fig. 18. Photos of fresh and dried apple slices from Day-1.

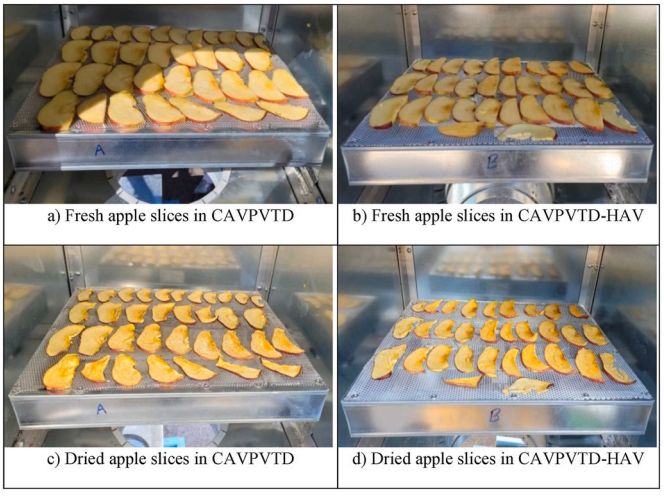

Fig. 19. Photos of fresh and dried apple slices from Day-2.

content of apple slices was 14.87 g water/g dry matter. The weight of samples was obtained every 30 s to finish the drying process at the final moisture content (MC). Apple slices lost moisture rapidly until 14:00 and then moisture loss decreased significantly. It was also observed from the data that when the drying temperature was high, the internal moisture migrating to the surface decreased rapidly with a faster rate of movement. As can be seen from the graphs, lower MC values were

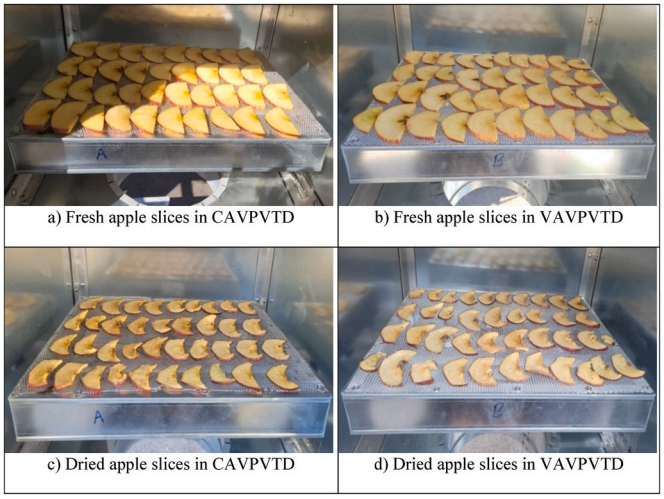

Fig. 20. Photos of fresh and dried apple slices from Day-3.

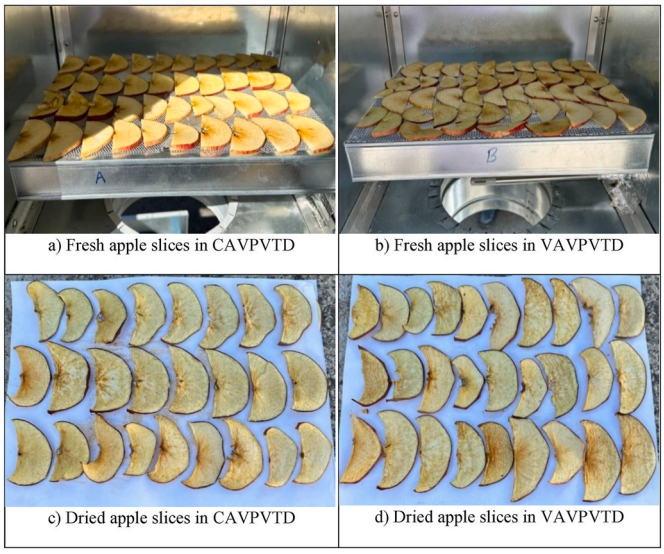

Fig. 21. Photos of fresh and dried apple slices from Day-4.

formed in CAVPVTD-HAV during the experiments on Day-1 and Day-2 due to the higher air volume flowing over the product and lower drying air temperature. In contrast, VAVPVTD outperformed on Day-3 and Day-4 by 9.68 % and 5.91 %, respectively.

Fig. 17 shows how instantaneous DR changes over time. The increase in drying temperature and airflow caused an increase in heat transfer in the product, which increased the vapor pressure in the apple slices, which is one of the driving forces of the water diffusion process, and increased the drying rate. The drying rate at the beginning of the experiment was observed to be higher due to the high internal and surface moisture and the decreasing rate of the drying period, after which the moisture evaporation decreased due to the decrease in this drying rate.

Figs. 18–21 show day-by-day photographs of fresh and dried apple slices. The photographs depict how the apple slices alter over time, shrinking and changing color as they dry. Dried product quality in terms of shrinkage and color visuality varied depending on environmental conditions. As the outside air temperature increased, the drying air temperature increased and accordingly the dried apple slices dried faster but shrinkage increased.

5. Conclusion

Two PVTD systems, one flat type with homogeneous air distribution with CAV and the other CAV, were created and tested for four days. The air volume was controlled according to the PV surface temperature with an algorithm created for VAV, the constant air volume PVTD performance was compared, and the following findings were obtained.

The average outlet air temperature of CAVPVTD was 4.2 %, 4.06 %, 2.85 %, and 2.64 % higher than CAVPVTD-HAV and VAVPVTD, from Day-1 to Day-4, respectively, which means that drying is done at higher temperatures. When comparing average efficiencies, the highest level of thermal efficiency was 32.28 % in CAVPVT on Day 4, whereas the highest electrical efficiency was 11.14 % in VAVPVTD on the same day. This is because better cooling is achieved in the VAV system. When the systems were examined for electricity efficiency, the VAVPVTD system outperformed the other by 12.06 %. When the systems were assessed for thermal efficiency, the CAVPVTD system outperformed the other by 9.9 %. This was due to the increased air volume in the VAV system achieving lower outlet air temperature. Because of the high outdoor air and surface temperatures in the VAV-controlled system, the algorithm boosted fan power consumption to maximum values, resulting in a COP value that was always lower than the system with constant air volume. In terms of COP, it is believed that the air volume value specified in the CAV system is optimal. When comparing the average effective diffusivity coefficients, they varied between $4.8 \times 10{-}7\ m^2/s$ and $7.75 \times 10{-}7\ m^2/s$. When the final MCs of dried apple slices were compared, VAVPVTD outperformed on Day-3 and Day-4 by 9.68 % and 5.91 %, respectively.

Consequently, for the studied systems and circumstances, the VAVPVTD performed well in terms of electrical efficiency but somewhat worse in terms of thermal efficiency and significantly poorer in terms of coefficient of performance. Considered from another perspective, it was observed that VAV control and novel design applications increased electrical efficiency by up to 12.06 % and shortened the drying time. On the other hand, PVT showed lower performance in thermal efficiency, up to 9.9 %. Furthermore, VAVPVTD performed up to 10 % better in terms of drying effectiveness. In this study, the algorithm acting according to the surface temperature tried to control the surface temperature of the PVT at 40 °C. Seasonal weather, depending on the conditions, can be tried to be controlled at different surface temperatures or depending on the PVT outlet air temperature.

PVT design is not suitable for use in natural conditions; it can be made suitable in the future. Higher surface temperatures have occurred in the lower middle area of the PVT compared to other areas; work can be done to prevent this. Fans reach maximum speeds in the VAV control state, and a fan with appropriate capacity and efficiency can be selected. Drying cabinets can be designed to reduce heat losses. By filtering the data that has been collected over a lengthy period, a more precise control mechanism can be constructed, which will result in a smoother measurement. Furthermore, the fan motor speed was controlled in ten different speed ranges; however, extending this range would allow for more exact flow ranges to be achieved.

CRediT authorship contribution statement

Fazlı Bayrak: Writing – original draft, Investigation, Conceptualization. **Mustafa Aktaş:** Writing – original draft, Supervision, Methodology, Investigation, Data curation, Conceptualization. **Ahmet Aktaş:** Writing – original draft, Validation, Software, Formal analysis, Conceptualization. **Seyfi Şevik:** Writing – review & editing, Writing – original draft, Supervision, Methodology, Investigation, Formal analysis, Conceptualization. **Burak Aktekeli:** Writing – original draft, Resources, Investigation, Conceptualization. **Yaren Güven:** Writing – original draft, Resources, Investigation, Conceptualization.

Declaration of competing interest

The authors declare that they have no known competing financial interests or personal relationships that could have appeared to influence the work reported in this paper.

References

[1] E. Sarı, Y. Güven, M. Aktaş, Solar powered eco design timber drying system, J. Polytech. 27 (4) (2024) 1473–1489.
[2] M. Koşan, G. Karaca Dolgun, B. Aktekeli, K. Saçılık, M. Aktaş, Design and analysis of new solar-powered sustainable dryers: alfalfa crop, J. Food Process. Eng. 46 (3) (2022) e14253.
[3] E. Arslan, M. Aktaş, 4E analysis of infrared-convective dryer powered solar photovoltaic thermal collector, Sol. Energy 208 (2020) 46–57.
[4] D. Velić, M. Planinić, S. Tomas, M. Bilić, Influence of airflow velocity on kinetics of convection apple drying, J. Food Eng. 64 (1) (2004) 97–102.
[5] P. Barnwal, G.N. Tiwari, Grape drying by using hybrid photovoltaic-thermal (PV/T) greenhouse dryer: an experimental study, Sol. Energy 82 (12) (2008) 1131–1144.
[6] D. Kong, Y. Wang, M. Li, V. Keovisar, M. Huang, Q. Yu, Experimental study of solar photovoltaic/thermal (PV/T) air collector drying performance, Sol. Energy 208 (2020) 978–989.
[7] M. Fterich, M.I. Elamy, E. Touti, H. Bentaher, Experimental and numerical study of tomatoes drying kinetics using solar dryer equipped with PVT air collector, Engineering Science and Technology, an International Journal 47 (2023) 101524.
[8] A. Gupta, A. Biswas, B. Das, B.V. Reddy, Development and testing of novel photovoltaic-thermal collector-based solar dryer for green tea drying application, Sol. Energy 231 (2022) 1072–1091.
[9] A. Gupta, B. Das, J.D. Mondol, Experimental and theoretical performance analysis of a hybrid photovoltaic-thermal (PVT) solar air dryer for green chillies, Int. J. Ambient Energy 43 (1) (2020) 2423–2431.
[10] M. Dorouzi, H. Mortezapour, H.R. Akhavan, A.G. Moghaddam, Tomato slices drying in a liquid desiccant-assisted solar dryer coupled with a photovoltaic-thermal regeneration system, Sol. Energy 162 (2018) 364–371.
[11] A. Gupta, B. Das, A. Biswas, J.D. Mondol, An environmental and economic evaluation of solar photovoltaic thermal dryer, Int. J. Environ. Sci. Technol. 19 (2022) 10773–10792.
[12] D. Kong, Y. Wang, M. Li, J. Liang, X. Liu, G. Yin, Quality study on different parts of Panax notoginseng root drying with a hybrid drying system powered by a solar photovoltaic/thermal air collector and wind turbine, Energy 245 (2022) 123216.
[13] S. Tiwari, G.N. Tiwari, I.M. Al-Helal, Performance analysis of photovoltaic–thermal (PVT) mixed mode greenhouse solar dryer, Sol. Energy 133 (2016) 421–428.
[14] M. Fterich, H. Chouikhi, H. Bentaher, A. Maalej, Experimental parametric study of a mixed-mode forced convection solar dryer equipped with a PV/T air collector, Sol. Energy 171 (2018) 751–760.
[15] J. Hu, J. Bi, W. Wang, X. Li, Comparison of characterization and composition of melanoidins from three different dried apple slices, Food Chem. 455 (2024) 139890.
[16] M. Daş, E.K. Akpınar, Determination of thermal and drying performances of the solar air dryer with solar tracking system: apple drying test, Case Stud. Therm. Eng. 21 (2020) 100731.
[17] M. Beigi, Hot air drying of apple slices: dehydration characteristics and quality assessment, Heat Mass Tran. 52 (2016) 1435–1442.
[18] E.K. Akpınar, A. Midilli, Y. Biçer, Thermodynamic analysis of the apple drying process, Proc. IME E J. Process Mech. Eng. 219 (1) (2005) 1–14.
[19] U. Baysan, A.I. Harun, M. Koç, Evaluation of innovative drying approaches in celery drying considering product quality and drying energy efficiency, Innov. Food Sci. Emerg. Technol. 93 (2024) 103636.
[20] A.A. Laskar, M. Ahmed, D.V.N. Vo, A. Abdullah, M. Shahadat, M.H. Mahmoud, M. Yusuf, Mathematical modeling and regression analysis using MATLAB for optimization of microwave drying efficiency of banana, Therm. Sci. Eng. Prog. 46 (2023) 102157.
[21] A. Aktaş, M. Koşan, B. Aktekeli, Y. Güven, E. Arslan, M. Aktaş, PVT using a variable air volume control algorithm, Energy 307 (2024) 132793.
[22] G. Karaca, E.C. Dolgun, M. Koşan, M. Aktaş, Photovoltaic-Thermal solar energy system design for dairy industry, Journal of Energy Systems 3 (2) (2019) 86–95.
[23] H. Fang, N. Zhang, G. Cai, H. Chen, J. Ma, D. Wu, T. Du, Y. Wang, Operation strategy optimization and heat transfer characteristic analysis of photovoltaic/thermal module series connected with flat plate solar collector: system experimental study, Renew. Energy 229 (2024) 120770.
[24] M. Aktaş, S. Şevik, H. Doğan, M. Öztürk, Drying of tomato in a photovoltaic and thermal solar-powered continuous dryer, J. Agric. Sci. 18 (2012) 287–298.
[25] D. Zare, S. Minaei, M.M. Zadeh, M.H. Khoshtaghaza, Computer simulation of rough rice drying in a batch dryer, Energy Convers. Manag. 47 (18–19) (2006) 3241–3254.
[26] M. Aktaş, M.Ç. Kara, Sliced kiwi drying in a solar energy and heat pump dryer, Journal of the Faculty of Engineering and Architecture of Gazi University 28 (4) (2014) 733–741.
[27] G. Karaca, E.C. Dolgun, M. Aktaş, Design of a new energy efficient and hygienic system for drying honey, J. Polytech. 23 (3) (2020) 713–719.
[28] M. Aktaş, A. Khanlari, A. Amini, S. Şevik, Performance analysis of heat pump and infrared–heat pump drying of grated carrot using energy-exergy methodology, Energy Convers. Manag. 132 (2017) 327–338.
[29] M. Aktaş, A. Khanlari, B. Aktekeli, A. Amini, Analysis of a new drying chamber for heat pump mint leaves dryer, Int. J. Hydrogen Energy 42 (28) (2017) 18034–18044.
[30] M. Aghbashlo, H. Mobli, S. Rafiee, A. Madadlou, Energy and exergy analyses of the spray drying process of fish oil microencapsulation, Biosyst. Eng. 111 (2) (2012) 229–241.
[31] M. Aktaş, S. Şevik, E.C. Dolgun, B. Demirci, Drying of grape pomace with a double pass solar collector, Dry. Technol. 37 (2019) 105–117.
[32] R. Yamankaradeniz, İ. Horuz, S. Coşkun, Ö. Kaynaklı, N. Yamankaradeniz, Air Conditioning Principles and Applications, fourth ed., Dora Publications, 2021, p. 21. Turkish.
[33] S.J. Babalis, E. Papanicolau, N. Kyriakis, V.G. Belessiotis, Evaluation of thin-layer drying models for describing drying kinetics of figs (Ficus carica), J. Food Eng. 75 (2) (2006) 205–214.
[34] M. Aktaş, E. Gönen, Bay leaves drying in a humidity controlled heat pump dryer, Journal of the Faculty of Engineering and Architecture of Gazi University 29 (2) (2014) 433–441.
[35] İ. Dinçer, M.M. Hussain, Development of a new Bi–Di correlation for solids drying, Int. J. Heat Mass Tran. 45 (15) (2002) 3065–3069.
[36] İ. Dinçer, Development of a new number (the Dincer number) for forced-convection heat transfer in heating and cooling applications, Int. J. Energy Res. 20 (1996) 419–422.
[37] J.P. Holman, Experimental Methods for Engineers, McGraw-Hill, USA, New York, 1966.